

# POLITECNICO DI TORINO

Corso di Laurea Magistrale in Ingegneria Meccanica LM33

Tesi di Laurea Magistrale

## Use of SED approach to predict the fatigue behaviour of Aluminium V-Notched Samples



### Relatore

Prof. Aurelio Soma'

Firma del relatore:

*A. Soma'*

### Correlatori

Prof. Filippo Berto

Firma correlatore:

*Filippo Berto*

Luigi Mario Viespoli

Firma correlatore:

*Luigi M. Viespoli*

### Candidato

Omar Shihadeh

Firma del candidato:

*Omar Shihadeh*

A.A. 2017/18



# Acknowledgments

I would first like to thank my thesis supervisor Prof. Aurelio Soma' of the Department of Mechanical and Aerospace Engineering at the Politecnico di Torino for choosing me among the many students of the class and giving me the possibility of joining this project at the NTNU University.

I would also like to acknowledge Prof. Filippo Berto of the Department of Mechanical and Industrial Engineering at the NTNU University as the second reader of this thesis. The door of his office was always open whenever I ran into a trouble spot or had a question about my research or writing. I really appreciated his help, especially during the most difficult moments, when I was stuck and the work was not going in the right direction. He gave me not only technical advices, but he also encouraged me and gave me the right confidence.

It has been a pleasure to work with Luigi and to know him as a researcher and as a friend. He devoted a lot of his time to help me, much more than he was expected to and I am gratefully indebted to him for his very valuable comments on this thesis. I really appreciated the fact he allowed me to stay in his house for a few days, at the very end of my work.

I would also like to thank the others researchers working and studying at the Department who had been always kind and very helpful.

I must express my very profound gratitude to my family and especially to my parents for providing me with unfailing support and continuous encouragement throughout my years of study and through the process of researching and writing this thesis. This accomplishment would not have been possible without them.

Finally I want to thank from the bottom of my heart Elisa, who helped me indeed in these three years. Without her help I would never have achieved the many goals I had set, since the bachelor's thesis until this last achievement. She has been my love, friend, both my model and assistant and I am so grateful to know her.

Author

Omar Shihadeh



# Contents

<b>TABLE OF FIGURES</b> .....	<b>7</b>
<b>ABSTRACT</b> .....	<b>9</b>
<b>1. A REVIEW ON FATIGUE LIFE PREDICTION METHODS</b> .....	<b>10</b>
1.1. STRESS-LIFE APPROACH (S-N) .....	10
1.2 MEAN STRESS EFFECTS .....	11
1.3 S-N CURVE REPRESENTATION AND APPROXIMATIONS .....	15
1.4 NOTCH STRESS INTENSITY FACTOR .....	16
1.5 STRAIN ENERGY DENSITY .....	21
1.6 ADVANTAGES OF USING SED METHOD .....	24
1.7 PARIS` LAW .....	28
<b>2. COMPUTATION OF STRAIN ENERGY DENSITY FOR V-NOTCHED ALUMINUM SAMPLES</b> .....	<b>32</b>
<b>3. DIFFERENCE BETWEEN ELASTIC AND PLASTIC MODEL</b> .....	<b>39</b>
<b>4. COMPUTATION OF THE NOTCH STRESS INTENSITY FACTOR</b> .....	<b>47</b>
<b>5. DIMENSIONLESS PARAMETER Y</b> .....	<b>52</b>
<b>6. INITIATION AND PROPAGATION OF THE CRACK</b> .....	<b>54</b>
<b>7. HAIGH DIAGRAM</b> .....	<b>59</b>
<b>8. EQUIVALENT METHOD TO CHARACTERIZE THE FATIGUE BEHAVIOR OF THE ALUMINUM SPECIMEN</b> .....	<b>68</b>
<b>9. CONCLUSION</b> .....	<b>74</b>
<b>APPENDIX A</b> .....	<b>76</b>
<b>APPENDIX B</b> .....	<b>78</b>
<b>APPENDIX C</b> .....	<b>81</b>
<b>APPENDIX D</b> .....	<b>83</b>
<b>BIBLIOGRAPHY</b> .....	<b>84</b>



# Table Of Figures

Figure 1 Typical S-N diagram (1) .....	10
Figure 2 S-N schematic of fatigue crack nucleation and fracture (1).....	11
Figure 3 Effect of mean stress on the fatigue life (6).....	13
Figure 4 Data fitting between gerber and goodman`s lines (1).....	14
Figure 5 Compressive and tensile effects (1).....	14
Figure 6 Cartesian (a) and polar (b) coordinate systems with stresses at the pointed v-notch tip (7) .....	17
Figure 7 Cylindrical control volume around pointed V-notch tip (9).....	21
Figure 8 Mean Value of SED for a Weld Toe Region (11).....	26
Figure 9 Reduction of the scatter band using mode I NSIF (12) .....	27
Figure 10 Typical crack growth behavior in constant amplitude fatigue loading (6) .....	29
Figure 11 Paris` Diagram (14).....	30
Figure 12 Geometry of the Specimen .....	32
Figure 13 Critical Area (sx) and Mesh of the Model (dx) .....	33
Figure 14 Wöhler curve of the Specimens loaded with R=0.....	34
figure 15 Wöhler curve of the specimens loaded with R=0.5.....	35
figure 16 Specimen 12, max load 50 MPa, fatigue life 511426 cycles, R=0.....	36
figure 17 Specimen 16,max load 50 MPa, fatigue life 532025 cycles, R=0.....	36
figure 18 Specimen 11, max load 120 MPa, fatigue life 16856 cycles, R=0.....	37
figure 19 Specimen 2, max load 120 MPa, fatigue life 16360 cycles, R=0.....	37
figure 20 Specimen 14, max load 80 MPa, fatigue life 653514 cycles, R=0.5.....	38
figure 21 Specimen 13, max load 120 MPa, fatigue life 116732 cycles, R=0.5.....	38
Figure 22 True stress-strain curve of aluminum alloy 6082-t6 (15).....	39
Figure 23 Equivalent Stress in the Elastic and Plastic model (120 MPa) .....	41
Figure 24 Equivalent Strain in the Elastic and Plastic model (120 MPa).....	42
Figure 25 Equivalent Stress in the Elastic and Plastic model (40 MPa) .....	43
Figure 26 Equivalent Strain in the Elastic and Plastic model (40 MPa).....	44
Figure 27 Stress vs time in a node close to the notch tip .....	45
Figure 28 Convergence study .....	46
Figure 29 Shape functions $\epsilon_1$ and $\epsilon_2$ versus the notch opening angle (9) .....	47
figure 30 Plot of stress in function of the distance from the tip .....	48
Figure 31 Plot of NSIF in function of the distance from the tip .....	49
Figure 32 Comparison between refine and coarse mesh .....	50
Figure 33 Data Fitting in Welded Aluminum Scatter Band .....	51
Figure 34 Comparison between V-Notch and Crack and data Fitting for V-notch .....	53
Figure 35 SED in function of the length of the crack .....	55
Figure 36 SED in function of the number of cycles in semi-log plot.....	56
Figure 37 SED in function of the number of cycles in log-log plot.....	57
Figure 38 influence of SED on the propagation of the crack .....	58

Figure 39 Influence of SED on the initiation of the crack .....	58
Figure 40 Erroneous Wöhler Diagram .....	60
Figure 41 Variability of the final length of the crack in function of the stress applied for R=0.....	62
Figure 42 Experimental Values in the Haigh Diagram .....	63
Figure 43 Gerber`s Relation with SED.....	64
Figure 44 Gerber`s Relation with stress.....	64
Figure 45 Goodman`s relation with sed.....	66
Figure 46 Goodman`s relation with stress.....	66
Figure 47 Gereber`s relation on Stress .....	69
Figure 48 Goodman`s relation on Stress.....	70
Figure 49 Gereber`s relation on SED.....	72
Figure 50 Goodman`s relation on SED .....	73
Figure 51 Cartesian (a) and polar (b) coordinate systems with stresses at the crack tip (7).....	76
Figure 52 In-plane notch stress components at the rounded V-notch (7) .....	78



# Abstract

The thesis presents a review on the classical methods for predicting fatigue life, especially for what concern the theory necessary to develop the model and the computations of the second part of the work, with a particular focus on the Strain Energy Density method, developed by Berto, Lazzarin et al. and all its advantages.

The aim of the work is that of using SED approach to predict the fatigue behavior of the aluminum alloy 6082-T6. The following steps are made in order to develop the model necessary to reach this goal:

1. Fatigue tests of 15 aluminum V-notched specimens;
2. Implementation of the elastic model and plot of the Wöhler curves using SED;
3. Analysis of the differences between elastic and plastic models, developed using the FEM software Ansys;
4. Computation of the Notch Stress Intensity Factor using SED and stress and comparison of the numerical values;
5. Computation of the number of cycles necessary to nucleate and propagate the crack and definition of two equivalent parameters,  $C'$  and  $n'$ , useful to apply the Paris law to SED;
6. Plot of the Haigh diagrams using SED;
7. Use of the equivalent stress and SED, computed using Gerber and Goodman's relation.

# 1.A Review on Fatigue Life Prediction Methods

## 1.1. Stress-Life approach (S-N)

When fatigue test experiment are made, no distinction between crack nucleation and growth is made, but it can be done with special care and observation or measurement on particular specimens.

Stress concentration influence can be studied by machining the specimens in notches, holes, or grooves, careful alignment is needed for axial loaded specimens to minimize bending. (1)

In the following figures S is the applied nominal stress, usually taken as the alternating stress  $S_a$  and N is the number of cycles or life to failure, where failure is defined as fracture.

Less variability in life at the shorter lives and greater variability in life at the longer lives can be appreciated. The following figure shows a continuously sloping curve until  $10^6$  cycles, while it shows a “knee” after that. This has been found in only a few materials between  $10^6$  and  $10^7$  cycles, but most materials do not contain a knee even under carefully controlled environmental conditions. (1)

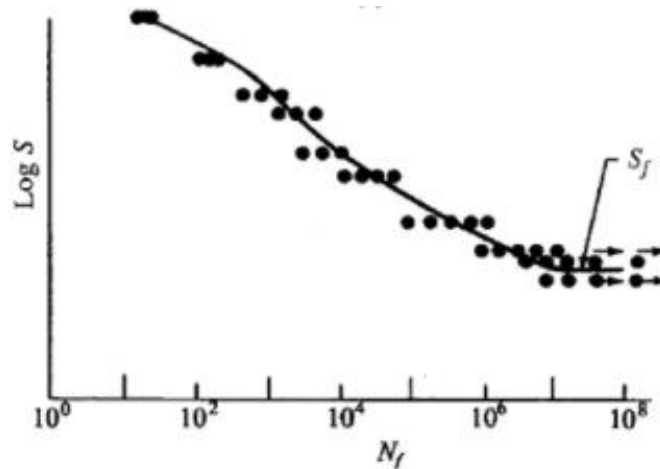


FIGURE 1 TYPICAL S-N DIAGRAM (1)

When sufficient data are taken at several stress levels, S-N curves are usually drawn through median lives and thus represent 50 percent expected failure. The fatigue life, N, is the number of cycles of stress or strain of a specified character that a given specimen sustains before failure of a specified nature occurs.

The number of cycles required to form the initial crack in smooth, unnotched or notched fatigue specimens and components can range from a small percentage to almost the entire life and a larger fraction of life for crack growth, occurs at higher stress levels, while a larger fraction of life for crack nucleation occurs at lower stress level (1).

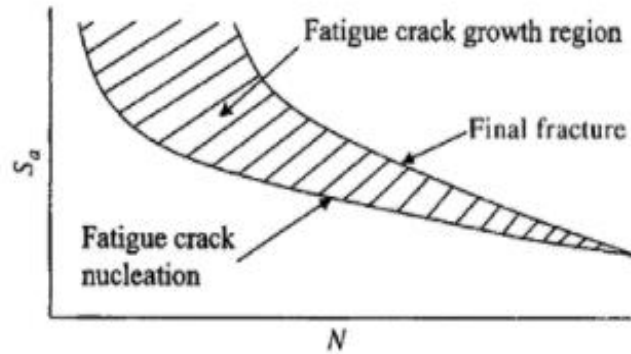


FIGURE 2 S-N SCHEMATIC OF FATIGUE CRACK NUCLEATION AND FRACTURE (1)

## 1.2 Mean Stress Effects

In order to model the effect of the mean stresses, a multitude of formulations have been proposed, most of which use the engineering tensile stress  $\sigma_{uts}$  or the monotonic yield stress  $\sigma_y$  as one of the parameters.

In general, these formulas come from empirical approaches to correlate groups of tests on particular materials, In fact in the literature it is widely documented that there is no general empirical law to relate the effect of mean stress on the fatigue limit (2).

Historically, the first tests of fatigue with mean stresses were performed by Wöhler and using his data, Gerber proposed in 1884 the following parabolic equation, known as the Gerber line or Relation (3), which was originally expressed through the following equation:

$$\sigma_a = \sigma_{-1} \left[ 1 - \left( \frac{\sigma_m}{\sigma_{uts}} \right)^2 \right] \quad (1.1)$$

It is a parabola, concave downward which passes through the point  $\sigma_{uts}$  on the x-axis and point  $\sigma_{-1}$  on y-axis with horizontal tangent. The sign of the mean stress has no influence on the alternating stress as it appears in squared form.

This equation was fitted with precision to the experimental data available at the time, when the tests with mean compression stresses were not possible (3).

As it was known that the mean compression loads are less damaging than the tensile ones, by proposing a symmetric method with respect to the mean stresses as the parabola, the results in compression would be on the safe side.

The work by O'Connor and Morrison in 1956 was the first investigation with machinery able to correctly apply compressive loads, showing a detrimental effect of the compressive mean stresses for some materials (3) and later investigations confirmed this fact.

For partly-brittle materials, the straight line is assumed as the best approximation. In 1922, the Goodman's theory (4) was modified by Haigh (5). The modified Goodman criterion can be expressed through this equation:

$$\sigma_a = \sigma_{-1} \left( 1 - \frac{\sigma_m}{\sigma_{uts}} \right) \quad (1.2)$$

Another commonly used empirical correlation corresponds to Dietmann, which is a parabola with axes parallel to x-axis, which equations is:

$$\sigma_a = \sigma_{-1} \sqrt{1 - \frac{\sigma_m}{\sigma_{uts}}} \quad (1.3)$$

This relationship shows a high statistical correlation with experimental data for tensile mean stresses due to the fact that is located between the lines of Goodman and Gerber for most of the range of the load ratio in axial mean stresses, where most of the experimental points are located according to some collections of data from the literature (3).

For compressive mean loads, the fatigue strength increases with the value of the compressive mean stress, showing a beneficial effect.

In contrast to the Gerber, Goodman and Dietmann empirical lines, some theories were developed on the basis of physical principles to explain the fatigue damage, but none of the energetic methods is able to successfully represent the fatigue behavior with superimposed static stresses.

Experimental results show that increasing the value of the tension mean stresses gradually reduces the axial stress amplitude the material can withstand without failure. This is shown in the following figure where alternating stress is plotted

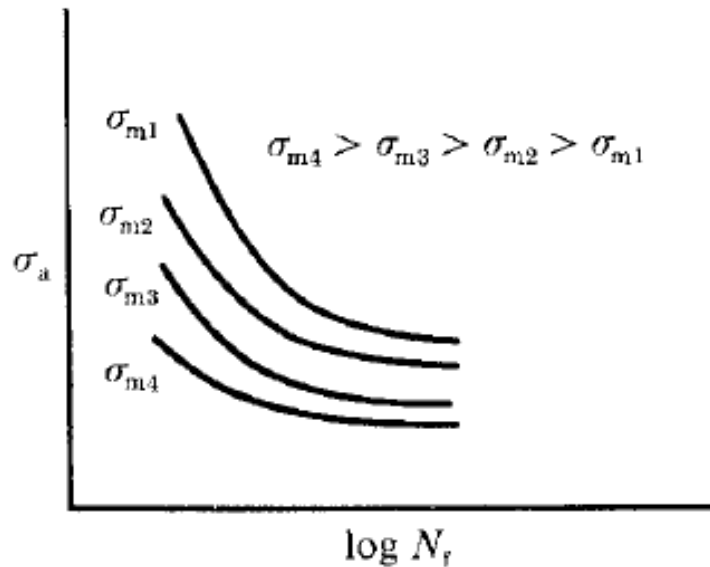


FIGURE 3 EFFECT OF MEAN STRESS ON THE FATIGUE LIFE (6)

It is seen that, in general, tensile mean stresses are damaging and compressive mean stresses are beneficial. Typical dimensionless plots are shown in the following figure for aluminum alloys, where  $S_a/S_f$  versus  $S_m/S_u$  is plotted.  $S_f$  is the fully reversed, fatigue limit of smooth specimens, and  $S_u$  is the ultimate tensile strength. Similar behavior exists for other alloys.

An evident scatter exists, but the general trend indicating that tensile mean stresses are detrimental is quite evident. Small tensile mean stresses, however, often have only a small effect. It appears that much of the data fall between the straight and curved lines. The straight line is the modified Goodman line, and the curve is the Gerber parabola

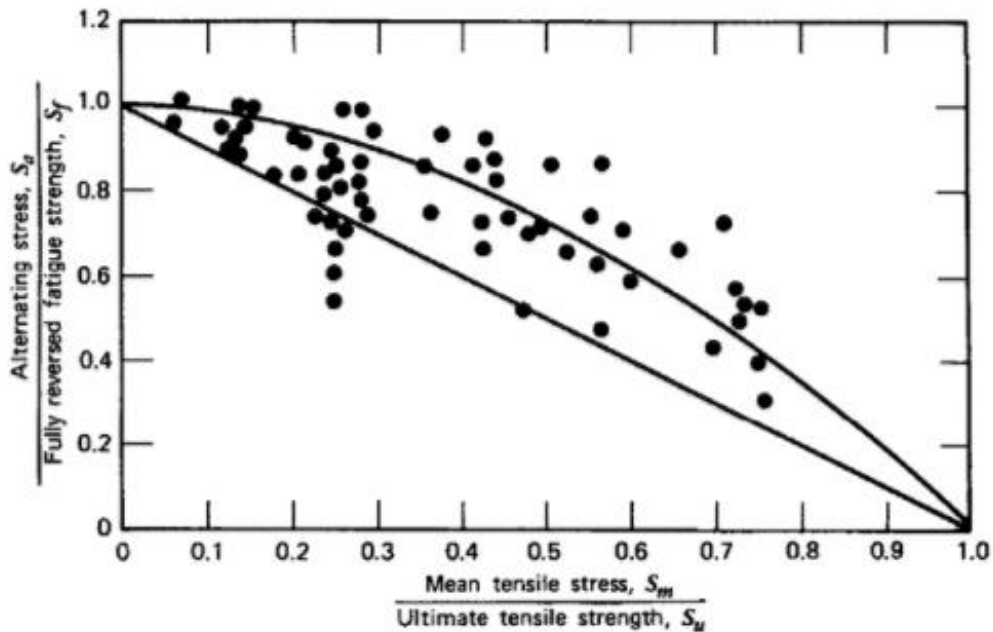


FIGURE 4 DATA FITTING BETWEEN GERBER AND GOODMAN'S LINES (1)

It is seen that these compressive mean stresses cause increases of up to 50 percent in the alternating fatigue strength and compressive residual stresses can cause similar beneficial behavior, resulting in a non-symmetrical Haigh diagram. The Gerber equation is incorrect, because it predicts a detrimental effect of compressive mean stresses and does not properly represent notched component tensile mean stress fatigue behavior.

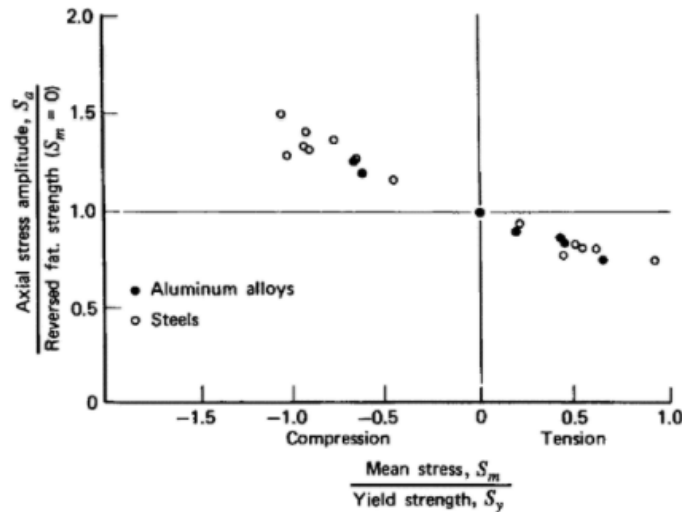


FIGURE 5 COMPRESSIVE AND TENSILE EFFECTS (1)

### 1.3 S-N Curve Representation and Approximations

Actual fatigue data from specimens or parts should be used in design if possible. This information may be available through data handbooks, company data files or previous tests, but it is often not available and must be generated or approximations of S-N behavior must be made (1).

Basquin in 1910 suggested a log-log straight line S-N relationship such that

$$S_a = A(N_f)^B \quad (1.4)$$

Where A is a coefficient and represents the value of  $S_a$  at one cycle, and B is the exponent or slope of the log-log S-N curve. One approximate representation of the S-N curve is a tri-slope model with one of them between 1 cycle and  $10^3$  cycles, one slope between  $10^3$  and  $10^6$  or  $10^8$  cycles, and another slope after  $10^6$  or  $10^8$  cycles, the third, or long-life, slope could also be horizontal. The tri-slope model indicates that a fatigue limit does not exist.

The surface effects are dominant at long fatigue lives and less significant at short lives, with convergence of the S-N curves at the monotonic ultimate tensile strength at  $N_f = 1$ . Different values of the slope, B, can be found for each surface condition. The convergence at  $N_f = 1$  is reasonable because surface finish does not have an appreciable effect on monotonic properties for most smooth metal specimens (1).

## 1.4 Notch Stress Intensity Factor

The stress intensity factor concept for describing the stress field at pointed crack or slit tips is well known from fracture mechanics.

The expressions of the stress distribution around the crack tip and those of the SIFs in the ligament ( $\theta = 0$ ) are given in the Appendix A.

Following the same logical passages done in Radaj (7) , the SIFs are substantially extended here in two directions. One extension refers to pointed V-notches with stress intensities depending on the notch opening angle and this is the case of the aluminum specimen studied in detail later in this work. Another extension refers to rounded notches with crack shape or V-notch shape and it is explain in detail in Appendix B. The loading mode related notch stress intensity factors  $K_1, K_2$  and  $K_3$  are introduced.

The asymptotic stress at the crack tip is described by the inverse square root of the radial distance  $r$  from the crack tip. A smaller, notch angle dependent exponent occurs in the case of corner notches, which means that the degree of the singularity is reduced.

The stress field close to corner can be described by stress intensity factors, these are named ‘notch stress intensity factors’ (NSIFs) as distinguished from the conventional stress intensity factors (SIFs) of crack tips.

The singular in-plane and out-of-plane stress fields at pointed corner notches can be specified by three notch loading modes (in analogy to the crack opening modes) related to the bisector plane of the notch: symmetric in-plane stresses (mode 1), antimetric in-plane stresses (mode 2) and out-of-plane shear stresses (mode 3). The corresponding notch loading modes are in-plane tensile loading, in-plane shear loading and out-of-plane shear loading.



The three basic loading modes with singular stresses at the notch tip produce the following asymptotic stress distribution around the notch tip, restricted to the first order terms. (7)

$$\sigma_{ij} = \frac{1}{\sqrt{2\pi}} [K_1 r^{\lambda_1-1} f_{1,ij}(\theta) + K_2 r^{\lambda_2-1} f_{2,ij}(\theta) + K_3 r^{\lambda_3-1} f_{3,kz}(\theta)] \quad (1.5)$$

(i, j = x, y and k = |x, y or i, j = r,  $\theta$  and k = r,  $\theta$ )

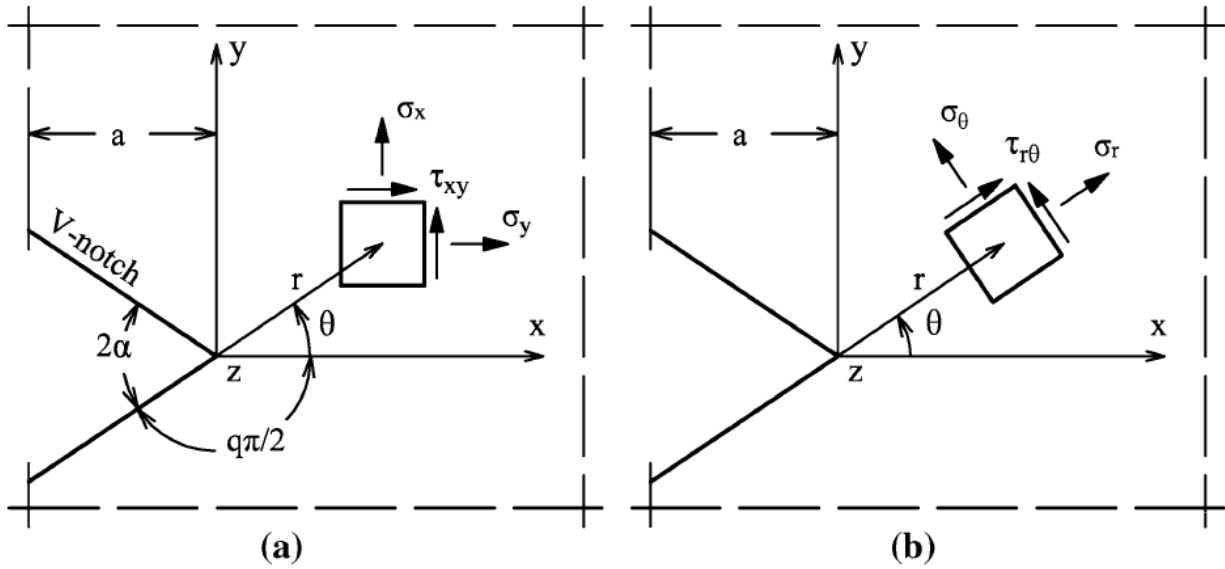


FIGURE 6 CARTESIAN (A) AND POLAR (B) COORDINATE SYSTEMS WITH STRESSES AT THE POINTED V-NOTCH TIP (7)

The NSIFs  $K_1, K_2$  and  $K_3$  depend on the magnitude of the load, the notch depth  $a$ , the notch opening angle  $2\alpha$  and further geometric parameters of the considered configuration. The angular functions  $f_{1,ij}, f_{2,ij}$  and  $f_{3,kz}$  describe the angular distribution of the stress close to the notch tip.

The exponent values for the stress distribution are the eigenvalues defined by the expression

$$\sin(\lambda_1 q\pi) + \lambda_1 \sin(q\pi) = 0 \quad (1.6)$$

$$\sin(\lambda_2 q\pi) + \lambda_2 \sin(q\pi) = 0 \quad (1.7)$$

Where ‘q’ is related to the opening angle by means of the expression  $2\alpha = \pi(2 - q)$ . Since  $2\alpha$  is a fixed parameter for a specific wedge or notch, the equation above provides the values of  $\lambda$ , called ‘eigenvalues’.

The stress field analysis for the V-notch subjected to out-of-plane shear loading (mode 3) is easier to perform and the next equation can be obtained

$$\sin \lambda_3(2\pi - 2\alpha) = 0 \quad (1.8)$$

The first non-zero eigenvalue is simply:

$$\lambda_3 = \frac{\pi}{2\pi - 2\alpha} \quad (1.9)$$

The in-plane stresses at the pointed V-notch are derived in the following form after introduction of the NSIFs  $K_1$  and  $K_2$  (7)

$$\begin{aligned} \begin{Bmatrix} \sigma_\theta \\ \sigma_r \\ \tau_{r\theta} \end{Bmatrix}_1 &= \frac{1}{\sqrt{2\pi}} \frac{r^{\lambda_1-1} K_1}{(1 + \lambda_1) + \chi_1(1 - \lambda_1)} \\ &\times \left[ \begin{Bmatrix} (1 + \lambda_1) \cos(1 - \lambda_1)\theta \\ (3 - \lambda_1) \cos(1 - \lambda_1)\theta \\ (1 - \lambda_1) \sin(1 - \lambda_1)\theta \end{Bmatrix} + \chi_1(1 - \lambda_1) \begin{Bmatrix} \cos(1 + \lambda_1)\theta \\ -\cos(1 + \lambda_1)\theta \\ \sin(1 + \lambda_1)\theta \end{Bmatrix} \right] \quad (1.10) \end{aligned}$$

$$\sigma_{z,1} = \nu(\sigma_{\theta,1} + \sigma_{r,1}) \quad (\text{plane strain})$$

$$\chi_1 = -\frac{\sin(1 - \lambda_1)q\pi/2}{\sin(1 + \lambda_1)q\pi/2}$$

$$\begin{aligned} \begin{Bmatrix} \sigma_\theta \\ \sigma_r \\ \tau_{r\theta} \end{Bmatrix}_2 &= \frac{1}{\sqrt{2\pi}} \frac{r^{\lambda_2-1} K_2}{(1 + \lambda_2) + \chi_2(1 - \lambda_2)} \\ &\times \left[ \begin{Bmatrix} -(1 + \lambda_2) \cos(1 - \lambda_2)\theta \\ -(3 - \lambda_2) \cos(1 - \lambda_2)\theta \\ (1 - \lambda_2) \sin(1 - \lambda_2)\theta \end{Bmatrix} + \chi_2(1 - \lambda_2) \begin{Bmatrix} -\sin(1 + \lambda_2)\theta \\ \sin(1 + \lambda_2)\theta \\ \cos(1 + \lambda_2)\theta \end{Bmatrix} \right] \quad (1.11) \end{aligned}$$

$$\sigma_{z,2} = \nu(\sigma_{\theta,2} + \sigma_{r,2}) \quad (\text{plane strain})$$

$$\chi_2 = -\frac{\sin(1 - \lambda_2)q\pi/2}{\sin(1 + \lambda_2)q\pi/2}$$

The anti-symmetrical singular and symmetrical non-singular out-of-plane shear stresses have the following form

$$\begin{aligned} \begin{Bmatrix} \tau_{rz} \\ \tau_{\theta z} \end{Bmatrix} &= \frac{1}{\sqrt{2\pi}} K_3 r^{\lambda_3-1} \begin{Bmatrix} \sin \lambda_3 \theta \\ \cos \lambda_3 \theta \end{Bmatrix} \\ \begin{Bmatrix} \tau_{rz} \\ \tau_{\theta z} \end{Bmatrix}_S &= S \begin{Bmatrix} \cos \theta \pi / (\pi - \alpha) \\ -\sin \theta \pi / (\pi - \alpha) \end{Bmatrix} \end{aligned} \quad (1.12)$$

The characteristic stress components in the bisector plane ( $\theta = 0$ ) have the following simple form:

$$\sigma_{\theta}(r, 0) = \frac{1}{\sqrt{2\pi}} K_1 r^{\lambda_1-1} \quad (1.13)$$

$$\tau_{r\theta}(r, 0) = \frac{1}{\sqrt{2\pi}} K_2 r^{\lambda_2-1} \quad (1.14)$$

$$\tau_{\theta z}(r, 0) = \frac{1}{\sqrt{2\pi}} K_3 r^{\lambda_3-1} \quad (1.15)$$

The NSIFs  $K_1, K_2$  and  $K_3$  may be evaluated on the basis of the characteristic stress components above considering the limit values for  $r \rightarrow 0$ .

$$K_1 = \lim_{r \rightarrow 0} \sqrt{2\pi} r^{1-\lambda_1} \sigma_{\theta}(r, 0) \quad (1.16)$$

$$K_2 = \lim_{r \rightarrow 0} \sqrt{2\pi} r^{1-\lambda_2} \tau_{r\theta}(r, 0) \quad (1.17)$$

$$K_3 = \lim_{r \rightarrow 0} \sqrt{2\pi} r^{1-\lambda_3} \tau_{\theta z}(r, 0) \quad (1.18)$$

It can be found, in a certain radius close to the notch tip, that the N-SIFs so calculated express a plateau at a certain value, which is a good estimate of the N-SIFs. The value obtained diverge from the plateau for small radius, not being the FEM results able to express the stress singularity, and far from the notch tip, where the remote stress field prevails on the stress intensification induced by the presence of the notch.

Only under very particular circumstances (components characterized by V-notches with a constant opening angle) can N-SIFs be directly used for predicting the static and fatigue behavior of components; otherwise, the variability of their dimensions does not allow it.

An energetic approach makes it possible to overcome the problem. In fact, physical dimensions of the strain energy density are  $\frac{Nmm}{mm^3}$ , independently of the opening angle.

This approach is explained in detail in the next paragraph.

### 1.5 Strain Energy Density

The local strain energy density (SED) approach is elaborated for strength assessments in respect of brittle fracture and high-cycle fatigue.

Whilst the NSIF evaluation needs very fine meshes in the vicinity of the points of singularity, which is a great drawback of the approach in the presence of complex geometries, the mean value of the elastic SED on the control volume can be accurately determined by using very coarse meshes.

The NSIF approach requires knowledge of the elastic stress field in the region very close to the notch tip. In order to achieve this using normal isoparametric elements, under a typical linear elastic hypothesis, FE meshes must be very refined in these regions (8).

The average SED in a defined control volume around the pointed or rounded notch (or crack) tip is considered to be the characteristic material parameter which describes the initiation of brittle fracture or high-cycle fatigue failure.

The approach is elaborated for pointed and rounded V-notches subjected to tensile loading.

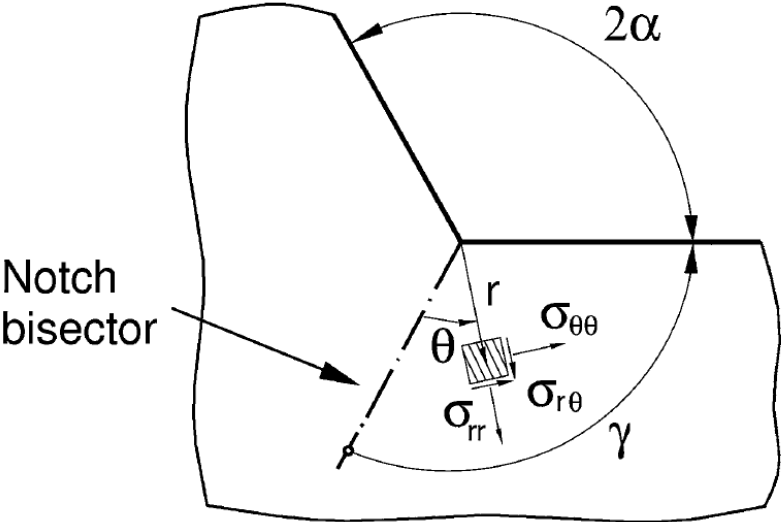


FIGURE 7 CYLINDRICAL CONTROL VOLUME AROUND POINTED V-NOTCH TIP (9)

The strain energy density  $W$  of in-plane stress fields can be expressed as follows:

$$W = \int_0^{\varepsilon_{ij}} \sigma_{ij} d\varepsilon_{ij} = \frac{1}{2} \sigma_{ij} \varepsilon_{ij} = \frac{1}{2} [\sigma_{\theta\theta} \varepsilon_{\theta\theta} + \sigma_{rr} \varepsilon_{rr} + \sigma_{zz} \varepsilon_{zz} + \sigma_{r\theta} \varepsilon_{r\theta}] \quad (1.19)$$

In the presence of a sharp V-shaped notch, the stress distributions of symmetric type with respect to the angle bisector (mode I) are those calculated previously for the N-SIF.

After some mathematical steps explained in detailed in the Appendix C the elastic deformation energy, averaged on the area  $A$ , turns out to be (9):

$$\bar{W} = \frac{E(R)}{A(R)} = \frac{1}{E} e_1 K_1^2 R^{2(\lambda_1-1)} + \frac{1}{E} e_2 K_2^2 R^{2(\lambda_2-1)} \quad (1.20)$$

Where:

$$e_1(2\alpha) = \frac{I_1(\gamma)}{4\lambda_1\gamma} \quad (1.21)$$

$$e_2(2\alpha) = \frac{I_2(\gamma)}{4\lambda_2\gamma} \quad (1.22)$$

$$A(R) = \int_0^R \int_{-\gamma}^{+\gamma} r dr d\theta = R^2 \gamma \quad (1.23)$$

Let us suppose that material failure occurs when the mean value of the deformation energy reaches a limit value characteristic of the material:

$$\bar{W} \leq W_C \quad (1.24)$$

If the material exhibits a brittle behavior, we have  $W_C = \sigma_R^2/2E$ .

The critical value of the radius, which is considered as a material property, can be determined on the basis of the toughness of the cracked component, containing a V-shaped notch with an opening angle equal to zero. When  $W_2$  is null (due to symmetry of geometry and loads) or it has a negligible value (as it happens, for example, in the presence of a great value of the opening angle that results in non singular stress distribution even in the presence of a V-shaped corner), the N-SIF can be directly correlated to the mean value of the energy  $W$ .

It is possible to obtain

$$K_1^n = \sqrt{\frac{4E\lambda_1\gamma}{I_1(\gamma)}} \bar{W} R^{(1-\lambda_1)} \quad (1.25)$$

At the critical conditions, substitution of  $\bar{W}$  with  $W_c$

$$K_{1c}^n = \sqrt{\frac{2\lambda_1\gamma}{I_1(\gamma)}} \sigma_R R^{(1-\lambda_1)} = f_1(2\alpha) \sigma_R R^{(1-\lambda_1)} \quad (1.26)$$

When the V-shaped notch becomes a crack, the value  $K_{1c}^n$  coincides with the toughness of a cracked body, so that

$$K_{1c}(0^\circ) = K_{IC} = f_1(0^\circ) \sigma_R R^{0.5} \quad (1.27)$$

As a consequence, the radius turns out to be:

$$R = \left( \frac{K_{IC}}{f_1(0^\circ) \sigma_R} \right)^2 \quad (1.28)$$

Finally, by substituting the expression of the radius in that of the toughness of the crack body, one obtains:

$$K_{1c}(2\alpha) = f_1(2\alpha) \sigma_R \left( \frac{K_{IC}}{f_1(0^\circ) \sigma_R} \right)^2 \quad (1.29)$$

Such expression makes it possible to evaluate the critical value of the parameter, characteristic of brittle material, against the opening angle  $2\alpha$ .

## 1.6 Advantages of using SED method

The displacement interpolation matrix  $[N]$  depends on the element type of the model and through this matrix it is possible to express the displacement vector  $\{u\}$  and the strain vector  $\{\varepsilon\}$  for a generic point belonging to the finite element. Then:

$$\{u\} = [N]\{d\} \quad (1.30)$$

$$\{\varepsilon\} = \frac{\partial\{u\}}{\partial x_i} = [B]\{d\} \quad (1.31)$$

In which:

$\{d\}$  is the vector of the nodal displacements

$[B]$  is the strain-displacement matrix

The rows of matrix  $[B]$  are obtained by appropriately differentiating the rows of the displacement interpolation matrix  $[N]$ .

Under linear elastic hypothesis, stresses are linked to strains by means of the well-known expression:

$$\{\sigma\} = [E]\{\varepsilon\} \quad (1.32)$$

Then, the strain energy density in a point P belonging to the finite element is:

$$W = \frac{1}{2}\{\varepsilon\}^t\{\sigma\} = \frac{1}{2}\{d\}^t[B]^t[E][B]\{d\} \quad (1.33)$$

Finally, the total strain energy stored in the finite element is

$$E_t = \int_V W dV = \frac{1}{2}\{d\}^t \left( \int_V [B]^t[E][B] dV \right) \{d\} = \frac{1}{2}\{d\}^t[K]\{d\} \quad (1.34)$$



This equation shows that the elastic strain energy  $E_t$  is directly determined from the nodal displacements, without any calculation involving stress and strains. Different from the strain energy evaluations, the stress evaluations need, as is well known, the derivatives of the displacements.

For this reason the mean value of the elastic SED on the control volume can be accurately determined by using relatively coarse meshes. This fact is of major importance for the applicability of the method to components of complex geometry, since the numerical models of this kind of structures quickly become large and time consuming when the local geometry is modelled for fatigue assessment. The structural stress method releases the requirements of small mesh sizes and normally needs a small fraction of the degrees of freedom as compared to those used for local methods (10).

The displacements and their derivatives must be continuous across the element boundaries. Obviously, this continuity does not necessarily implicate that the element stresses are continuous too. Stresses obtained at a node belonging to faced finite elements are very different when a coarse mesh is used. As a natural consequence, the degree of mesh refinement required for the accurate determination of the strain energy is much lower than that required for the stress fields, simply because in the former case no derivation or integration process is really involved (11).

It is possible to show a practical example that demonstrate the theory just explained by creating a FEM model and computing the different values of SED between a coarse mesh and a refine one.

This work has been done by Lazzarin, Berto and Zappalorto (11) for welded structures and the results summarized in the figure below have been obtained:

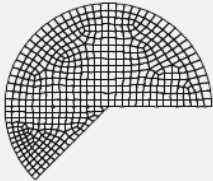
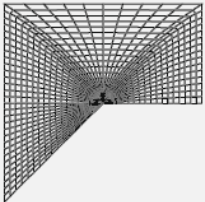
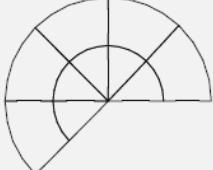
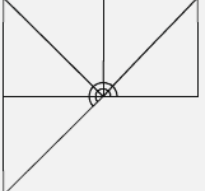
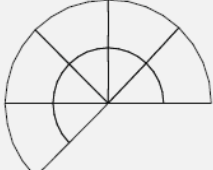
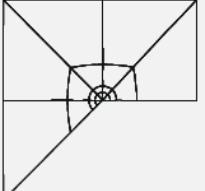
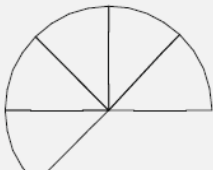
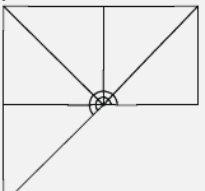
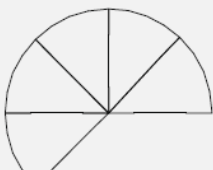
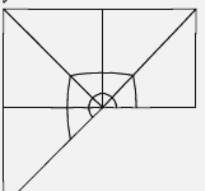
Number FE (full sector)	Weld toe $R_0 = 0.28$ mm		Number FE (model)	$\bar{W}_{FS}$ (MJ/m <sup>3</sup> )	$\Delta_{FS}$ (%)
475			19,555	0.04359	-
10			45	0.04909	+11.2
10			50	0.045199	+3.6
5			40	0.04898	+11.0
5			45	0.04519	+3.6

FIGURE 8 MEAN VALUE OF SED FOR A WELD TOE REGION (11)

As it is shown the mean value of SED does not vary much with the refinement of the mesh, in fact the difference between a model with 45 and 19555 elements is just 3.6%.

Another advantage of using this method is the possibility to reduce the scatter band of the Wöhler plot.

Due to large variations in the geometrical parameters, the scatter of the experimental data can be obviously very pronounced in terms of nominal stress range. The following figure shows that the scatter greatly decreases as soon as the mode I NSIF is used as a meaningful parameter for summarizing fatigue total life data.

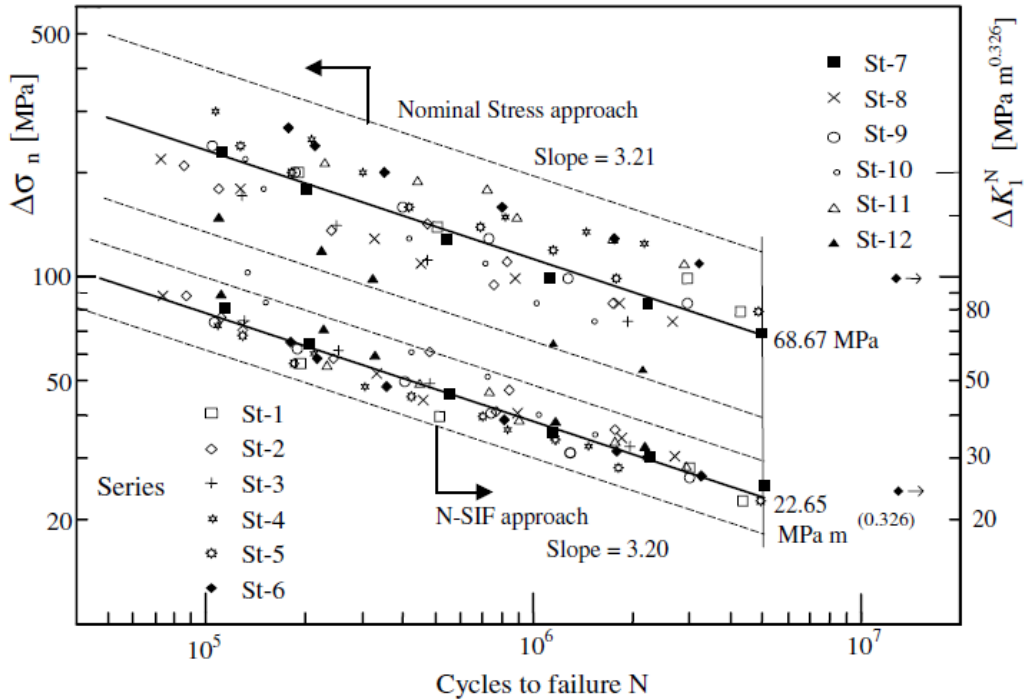


FIGURE 9 REDUCTION OF THE SCATTER BAND USING MODE I NSIF (12)

The original data are taken from the welded joints analyzed by Maddox (1987) and Gurney (1991), while the plot was made by Livieri and Lazzarin (2005).

From a theoretical point of view the NSIF-based band shown in this figure cannot be applied when the angle changes. That is simply because units for mode I NSIF are  $MPa \cdot m^\beta$ , where the exponent  $\beta$  depends on the V-notch angle.

This problem has been overcome by using the mean value of the strain energy density range present in a control volume of radius  $R_c$  surrounding the area near the stress concentration.

The strain energy density range was given in closed form as a function of the relevant NSIFs, whereas  $R_c$  is thought of as dependent on welded material properties (9).

## 1.7 Paris` Law

Classic fatigue design is usually based on Wöhler and Smith diagrams, but it is not always enough to keep the stress under the limit value, because of the defects of the components. For this reason a crack can initiate and propagate, till the component breaks. The useful fatigue life is calculated as the number of cycles to propagate a dominant defect of a measured initial size (or the largest undetected crack size estimated from the resolution of the inspection method) to a critical dimension. In most metallic materials, catastrophic failure is preceded by a substantial amount of stable crack propagation under cyclic loading conditions.

The most of the studies are focused on circumstances for which linear elastic fracture mechanics concepts are expected to be valid. Fatigue crack advance where considerably plastic nonlinear deformation occurs ahead of a crack tip or notch tip.

Data on the propagations of cracks are usually available for a null load ratio, in fact for any load ratio of the specimen, the compression tends to close the crack, so SIF does not exist. It has also been demonstrated from experiments that a stress of compression does not affect the crack.

The life of a component is obviously strongly dependent on the load, the geometry and the dimension of the crack at the beginning of its life, so for each combination of this variables and many others of less importance, such as the load ration and the temperature, the specimen has a different behavior.

The rate of growth of a fatigue crack subjected to constant amplitude stress reversals is expressed in terms of the crack length increment per cycle,  $da/dN$ . Values of  $da/dN$  for different loading conditions are defined from experimentally determined changes in crack length over a number of elapsed fatigue cycles (6).

One of the goals in fatigue design is to develop reliable methods for characterizing the crack growth rate in terms of an appropriate loading parameter which enables a quantification of the intrinsic resistance of the material to fatigue crack growth for different combinations of applied stresses, specimen geometry and crack geometry (6). When cyclic stresses applied to a component are so small that the zone of plastic deformation ahead of the advancing fatigue crack is a minor perturbation in an otherwise elastic field, linear elastic fracture mechanics solutions provide appropriate continuum descriptions for fatigue fracture. Paris & Erdogan (1963) suggested that for a cyclic variation of the imposed stress field, the linear elastic fracture mechanics characterization of the rate of fatigue crack growth should be based on the stress intensity factor range:

$$\Delta K = K_{max} - K_{min} \quad (1.35)$$

Knowing that

$$K = Y\sigma \sqrt{a} \quad (1.36)$$

$$\Delta K = Y\Delta\sigma \sqrt{a} \quad (1.37)$$

$$\Delta\sigma = \sigma_{max} - \sigma_{min} \quad (1.38)$$

Where  $Y$  is a geometrical factor which depends on the ratio between the crack length  $a$  and the width of the specimen  $W$ .  $\sigma_{max}$  and  $\sigma_{min}$  are the maximum and minimum values, respectively, of the fatigue stress cycle.

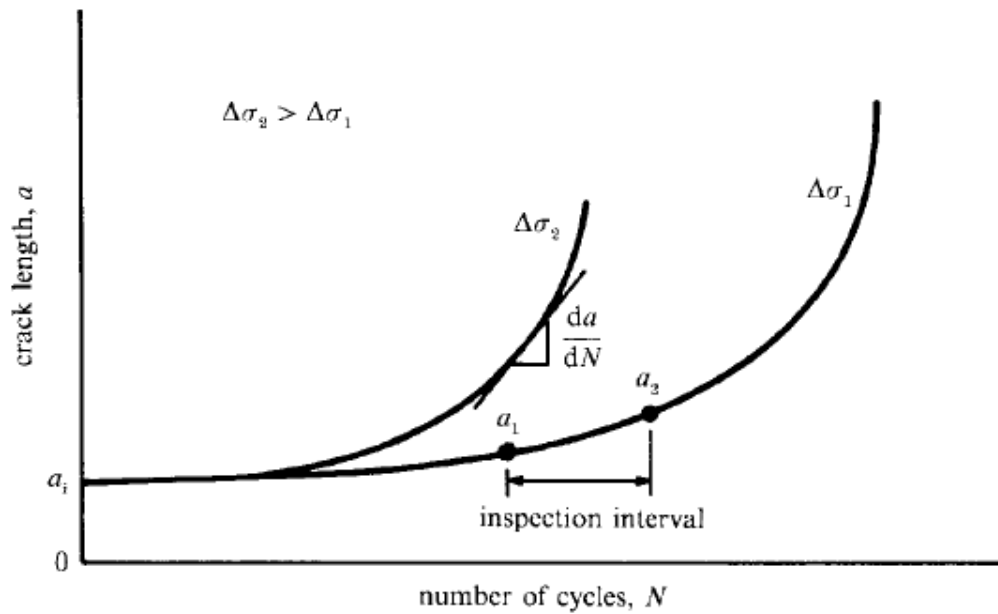


FIGURE 10 TYPICAL CRACK GROWTH BEHAVIOR IN CONSTANT AMPLITUDE FATIGUE LOADING (6)

For the first time in 1963 it was discovered by Paris and Erdogan that by plotting the fatigue crack growth increment  $da/dN$  versus the stress intensity factor on a log-log plot, they can be quite well fitted by a straight line.

They are therefore related by the well-known power law relationship (13)

$$\frac{da}{dN} = C \Delta K^n \quad (1.39)$$

Where C and n depend especially on the material and the load ratio.

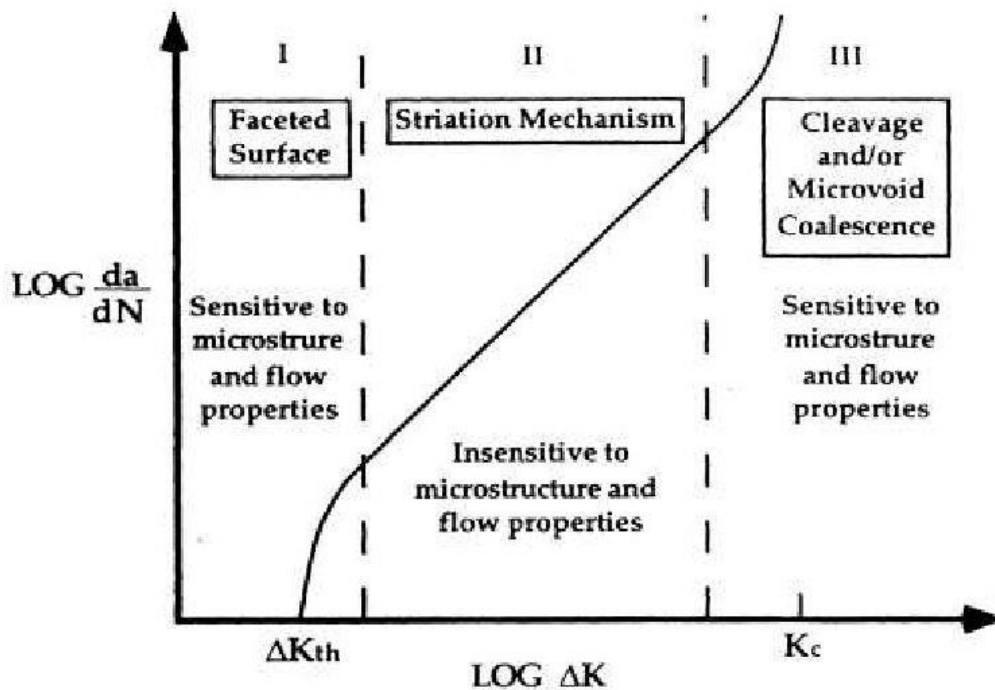


FIGURE 11 PARIS' DIAGRAM (14)

Although the fracture mechanics approach to fatigue crack growth was a subject of some controversy in the early 1960s, experimental data gathered for a wide range of metallic materials confirmed the power law relationship. Specifically, crack growth experiments on aluminum alloys with different combinations of stress range and crack length and with different specimen geometries unambiguously established the validity of such a characterization (6).

Although this equation is empirical, it has remained one of the most useful expressions in the analysis of fatigue crack growth for a vast spectrum of materials and fatigue test conditions.

It is important to note here that stable fatigue crack growth occurs at stress intensity factor levels that are well below the quasi-static fracture toughness,  $K_{Ic}$  in very ductile metallic materials.

The unique characterization of fatigue crack growth using the Paris law holds only for fixed values of the load ratio,  $R$ , and fixed environmental conditions. If environmental conditions, including temperature, have a strong effect on fatigue fracture, loading parameters such as cyclic frequency and waveform would also be expected to have a pronounced effect on crack growth rates.

Changes in these test conditions can lead to changes in the empirical constants  $C$  and  $m$  and in the fatigue crack growth rates. For fixed environmental conditions, one would then expect the crack growth to be strongly influenced not only by  $\Delta K$ , but also by the load ratio,  $R$ . This possibility then naturally gives rise to the notion that the general mechanical conditions governing fatigue crack growth are most accurately characterized by two parameters,  $\Delta K$  and  $R$ .

The simplicity of the Paris power law relationship provides a means of estimating the useful life of a fatigued component for design or failure analysis.

The fatigue life or the number of fatigue cycles to failure is calculated by integrating the Paris law from an assumed initial defect size  $a_0$  to a critical crack size  $a_f$ .

For a fixed value of the load ratio, if fatigue loading involves a constant amplitude of far-field stresses and a crack length change ( $a_f - a_0$ ) over which  $Y$  is roughly constant, the resulting fatigue life is

$$N = \int_{a_0}^{a_f} \frac{da}{C(Y\Delta\sigma\sqrt{a})^n} \quad (1.40)$$

And if  $n=2$

$$N = \frac{1}{CY^2\Delta\sigma^2} \log \frac{a_f}{a_0} \quad (1.41)$$

While if  $n \neq 2$

$$N = \frac{a_f^{1-n/2} - a_0^{1-n/2}}{(1 - n/2)CY^n\Delta\sigma^n} \quad (1.42)$$

## 2. Computation of Strain Energy Density for V-Notched Aluminum Samples

A static linear analysis has been performed, using the Ansys® APDL code, to compute the value of SED around the V-shaped notch's tip. It has been used a plane183 element in condition of plain strain. In the table below are reported the relevant value of the 6082-T6 aluminum alloy of the sample.

<b>E [MPa]</b>	<b><math>\nu</math></b>	<b><math>\sigma_R</math> [MPa]</b>
64000	0,34	275

The critical radius is assumed equal to that of the welded aluminum, which can be found in literature and it is equal to 0.12 mm (12). The geometry of the sample is reported in the following figure

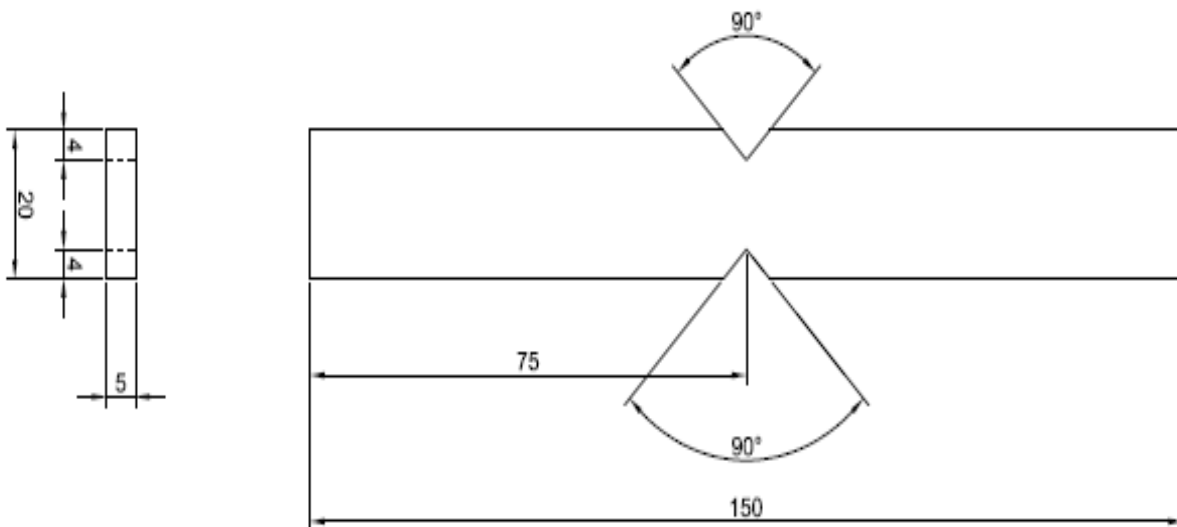


FIGURE 12 GEOMETRY OF THE SPECIMEN



In the Ansys' model the specimen has been loaded to ensure a tension  $\Delta\sigma_1$  of 1 MPa at the restricted area.

The averaged SED value on the control volume can be computed simply by dividing two outputs of the model

$$W = \frac{SENE}{VOLU} \tag{2.1}$$

In which SENE is the strain energy of the control volume and VOLU is the volume inside the critical radius.

As it is shown in the table and in the figure below, coarse mesh in enough to compute a precise value of SED. Singular elements around the notch's tip have been used, thanks to the command KSCON, which allows to move the nodes on the radial sides of the element at a quarter of the side length from the concentration point.

elements	volu [mm <sup>3</sup> ]	sene [N·mm]	$\Delta W_1$ [N·mm/mm <sup>3</sup> ]
142	1,696E-02	1,733E-06	1,021E-04
508	1,696E-02	1,725E-06	1,017E-04
1098	1,696E-02	1,725E-06	1,017E-04

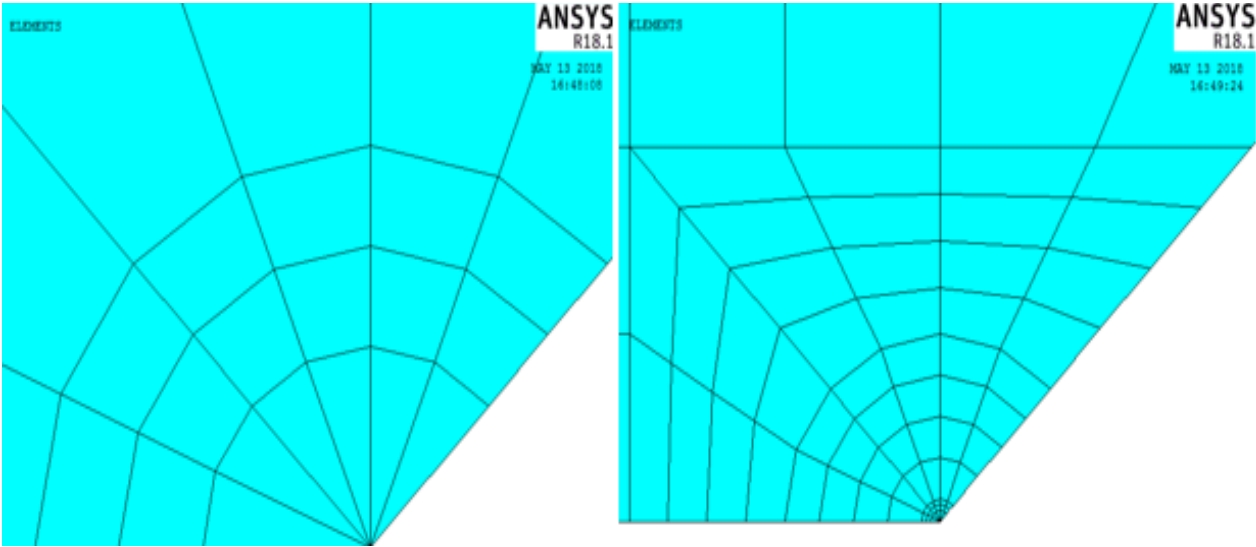


FIGURE 13 CRITICAL AREA (SX) AND MESH OF THE MODEL (DX)

Using the following expression, it is possible to evaluate the value of SED for each test and to plot its value in function of the number of cycles

$$W = \frac{SENE}{VOLU} \quad (2.2)$$

The Wöhler curve and the data for the two series of specimens with load ratio equal to 0 and 0.5 are

$\sigma_{max}$ [MPa]	N [cycle]	$\Delta W$ [N·mm/mm <sup>3</sup> ]
	RUN	
40	OUT	0,163
50	511426	0,254
50	532025	0,254
60	270174	0,366
60	298772	0,366
80	59360	0,651
80	86392	0,651
100	34745	1,017
100	35148	1,017
120	16360	1,465
120	16856	1,465

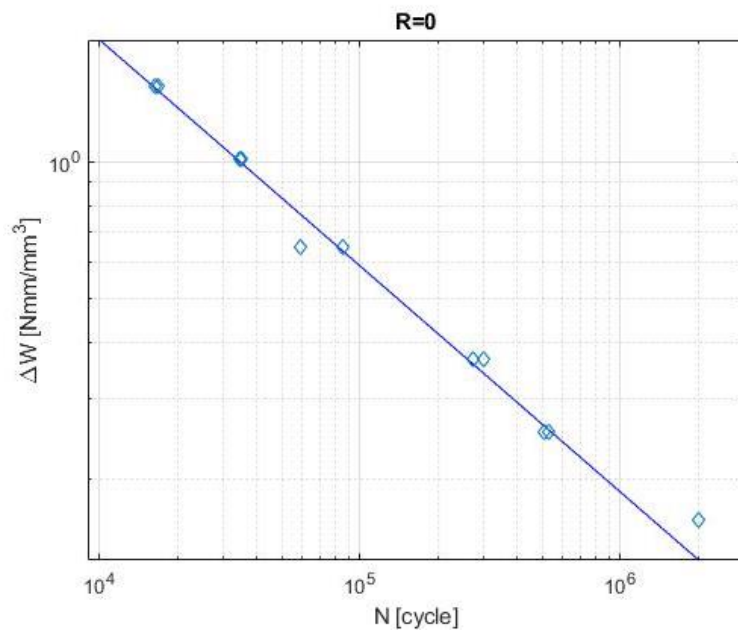
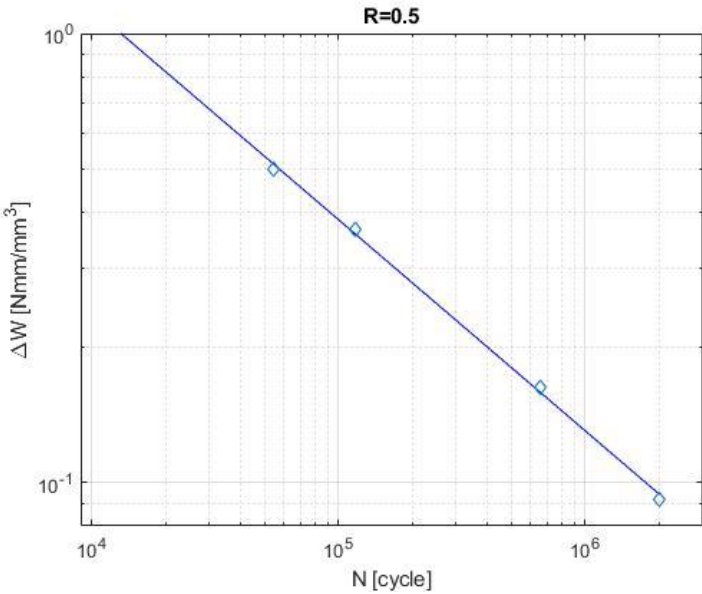


FIGURE 14 WÖHLER CURVE OF THE SPECIMENS LOADED WITH R=0

$\sigma_{max}$ [MPa]	N [cycle]	$\Delta W$ [N·mm/mm <sup>3</sup> ]
60	2000000	0,092
80	653514	0,163
120	116732	0.366
140	54631	0.498



**FIGURE 15 WÖHLER CURVE OF THE SPECIMENS LOADED WITH R=0.5**



FIGURE 16 SPECIMEN 12, MAX LOAD 50 MPA, FATIGUE LIFE 511426 CYCLES, R=0



FIGURE 17 SPECIMEN 16, MAX LOAD 50 MPA, FATIGUE LIFE 532025 CYCLES, R=0



**FIGURE 18 SPECIMEN 11, MAX LOAD 120 MPA, FATIGUE LIFE 16856 CYCLES, R=0**



**FIGURE 19 SPECIMEN 2, MAX LOAD 120 MPA, FATIGUE LIFE 16360 CYCLES, R=0**



**FIGURE 20 SPECIMEN 14, MAX LOAD 80 MPA, FATIGUE LIFE 653514 CYCLES, R=0.5**



**FIGURE 21 SPECIMEN 13, MAX LOAD 120 MPA, FATIGUE LIFE 116732 CYCLES, R=0.5**

### 3. Difference between Elastic and Plastic Model

The aim of this paragraph is to estimate the error committed in considering an elastic model instead of a plastic one while studying a V-sharp notch and computing SED.

The figure below shows the true stress strain curves of 6082-T6 aluminum alloy. The flow stress increased rapidly as the strain increased. When the stress reached a certain point, the material began to yield. After entering the plastic stage, under the effects of work-hardening and dynamic recovery, flow stress increased much slower than the beginning part. When the stress reached a certain value, the material began necking and local stress increased sharply (15).

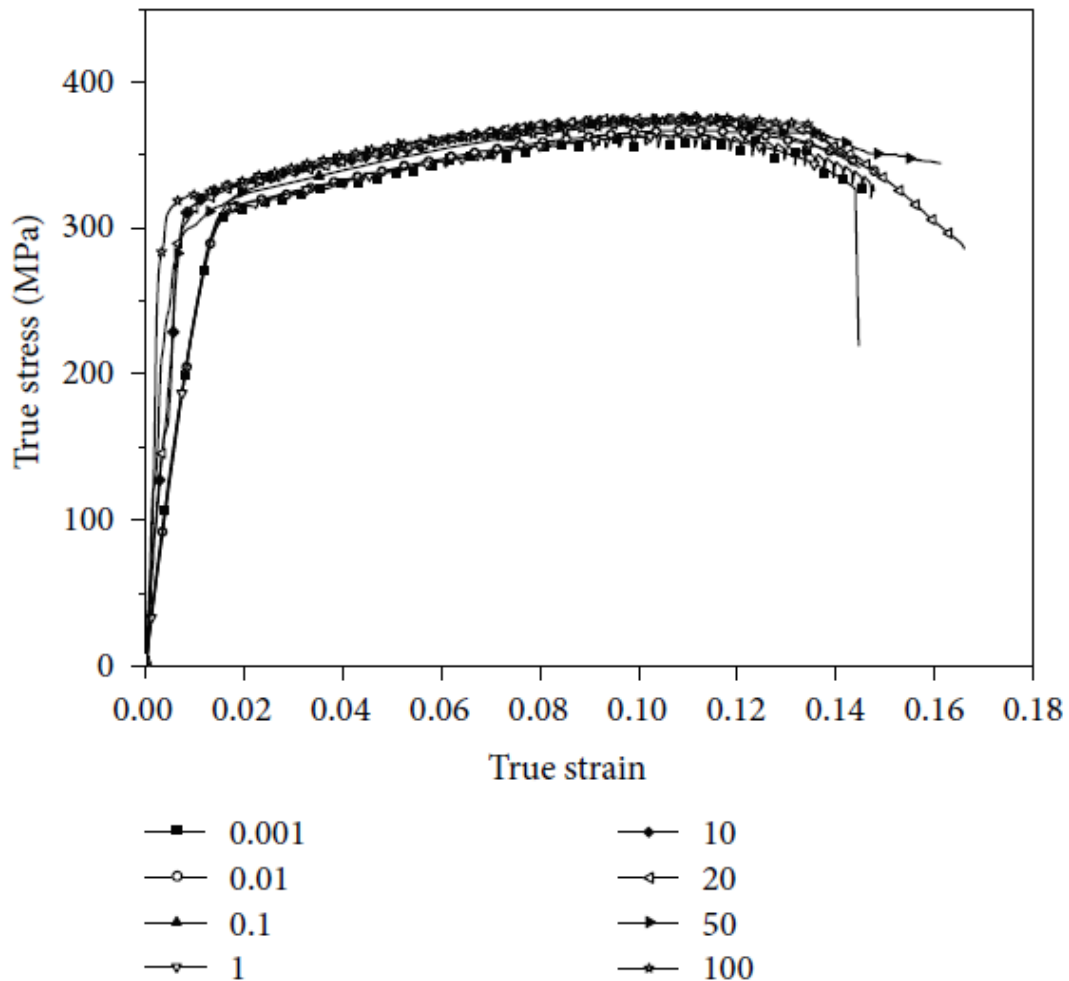


FIGURE 22 TRUE STRESS-STRAIN CURVE OF ALUMINUM ALLOY 6082-T6 (15)

This is the curve implemented in Ansys to compute the plastic model, from different value of the strain rate the material shows different value of the UTS and the yield stress.

Since the material showed no significant yield point, therefore the strain of 0.2% was used as the yield point. As the strain rate increased from  $0.001\text{s}^{-1}$  to  $100\text{ s}^{-1}$ , the yield stress increased from 306.1 MPa to 322.63 MPa, increased by 5.4%, and the tensile strength increased from 364 MPa to 384 MPa, increased by 5.49% (15). So an average value have been used, a yield stress of 315 MPa. The plastic part of the plot has been modelled using Johnson Cook law:

$$\sigma = A + B\epsilon_p^n \quad (3.1)$$

By fitting the experimental data the value of the constants are achieved (15):

$$A = 305.72$$

$$B = 304.9$$

$$n = 0.6796$$

The curve is plotted until a strain of 1, this is obviously absurd, but it is necessary to avoid errors near the notch tip, where the strain might be high for high value of the stress.

The mesh used is refine, even with SED, because the following is a plastic model, which needs to be studied with more precision than the elastic one. It is shown that a more precise model allows to obtain a better solution, but it is more complicated to compute.

Through Ansys it is possible to plot the equivalent stress and strain. In the following figures this plot is shown for a load of 120 MPa and 40 MPa and looking at the superior limit of the scale it is possible to notice that a plastic model shows higher strains than the elastic one, but the stress is obviously less because the materials yields.

All the plots are shown with the same mesh.



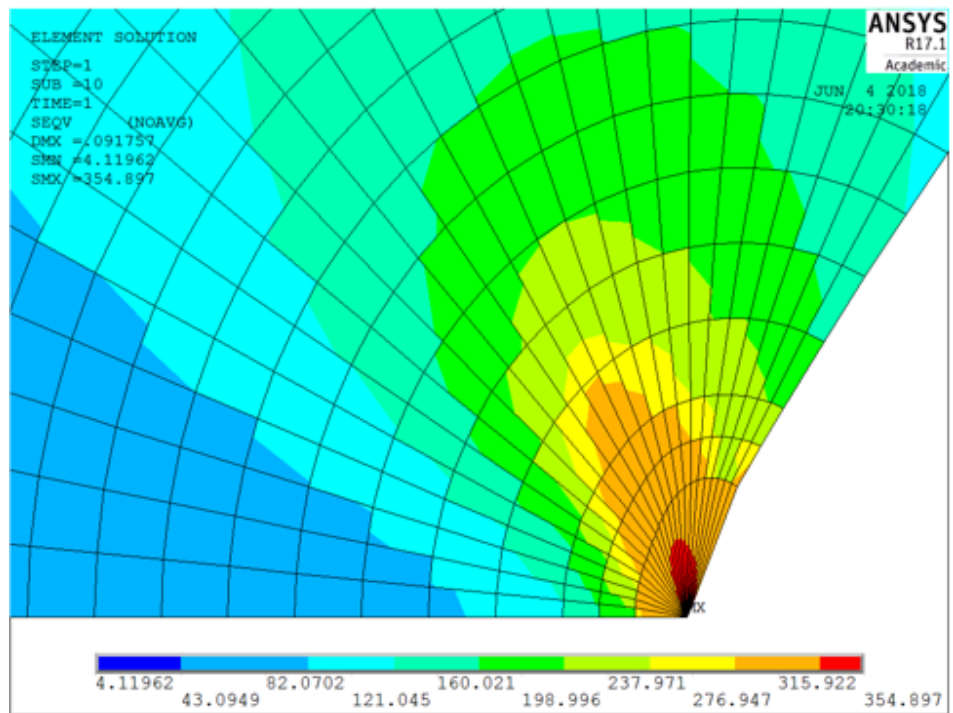
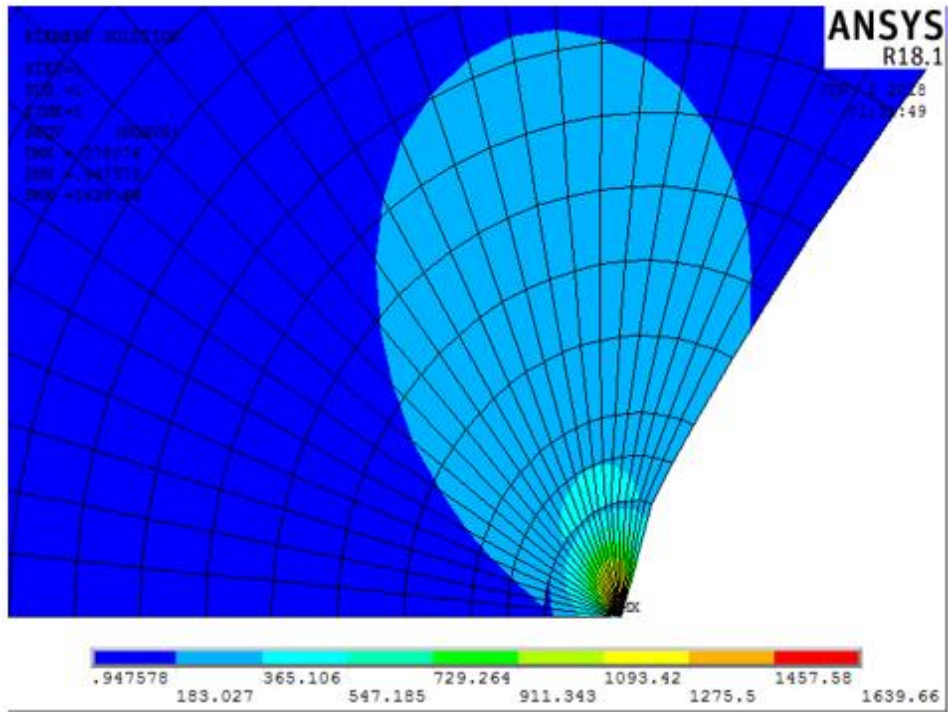


FIGURE 23 EQUIVALENT STRESS IN THE ELASTIC AND PLASTIC MODEL (120 MPa)

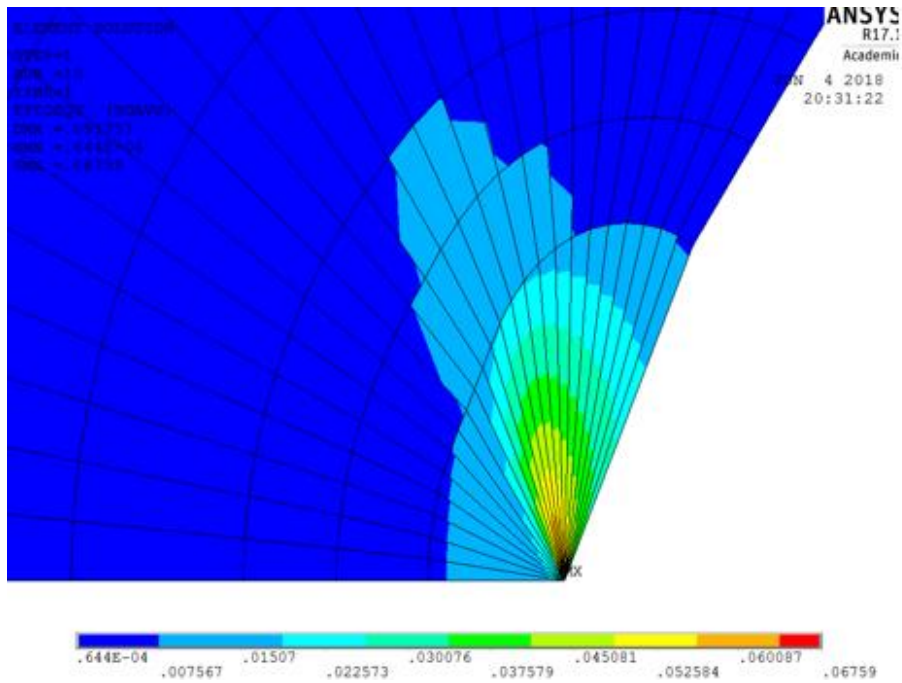
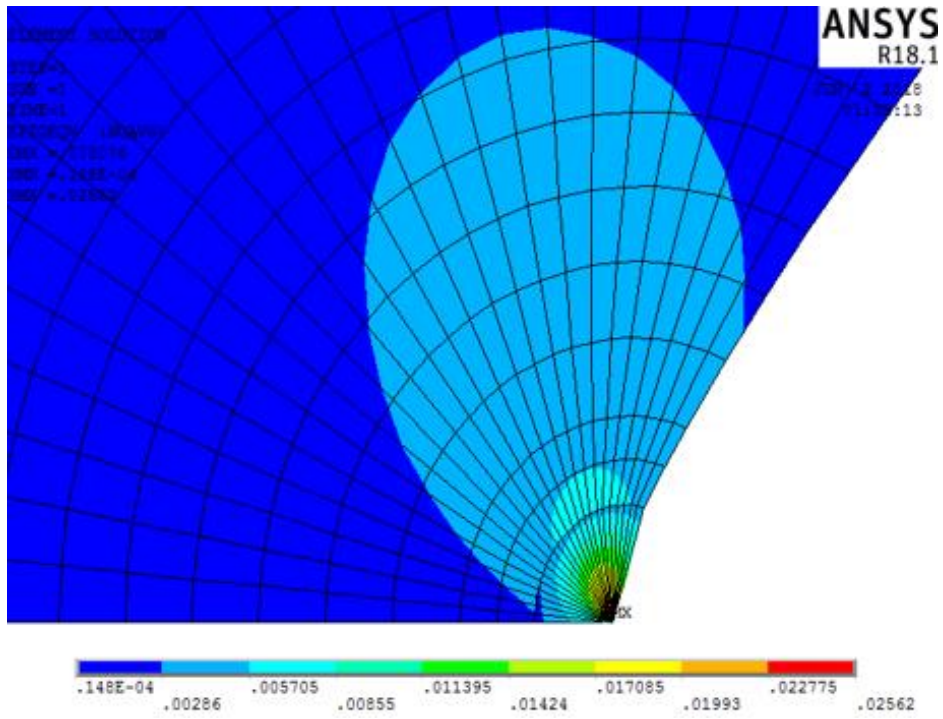


FIGURE 24 EQUIVALENT STRAIN IN THE ELASTIC AND PLASTIC MODEL (120 MPA)

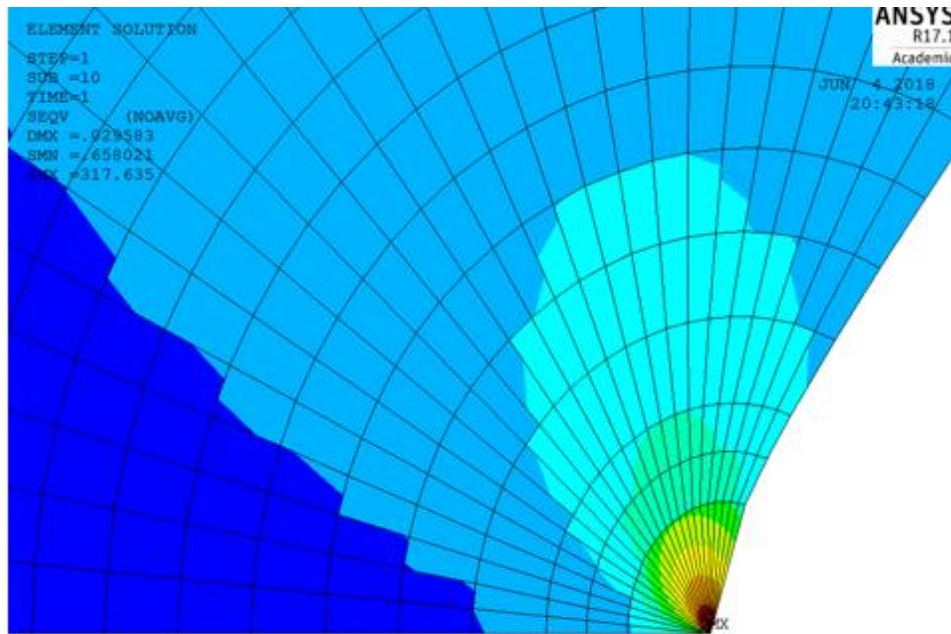
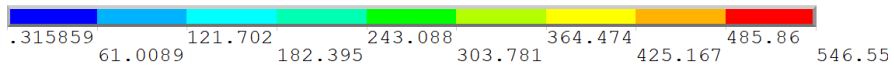
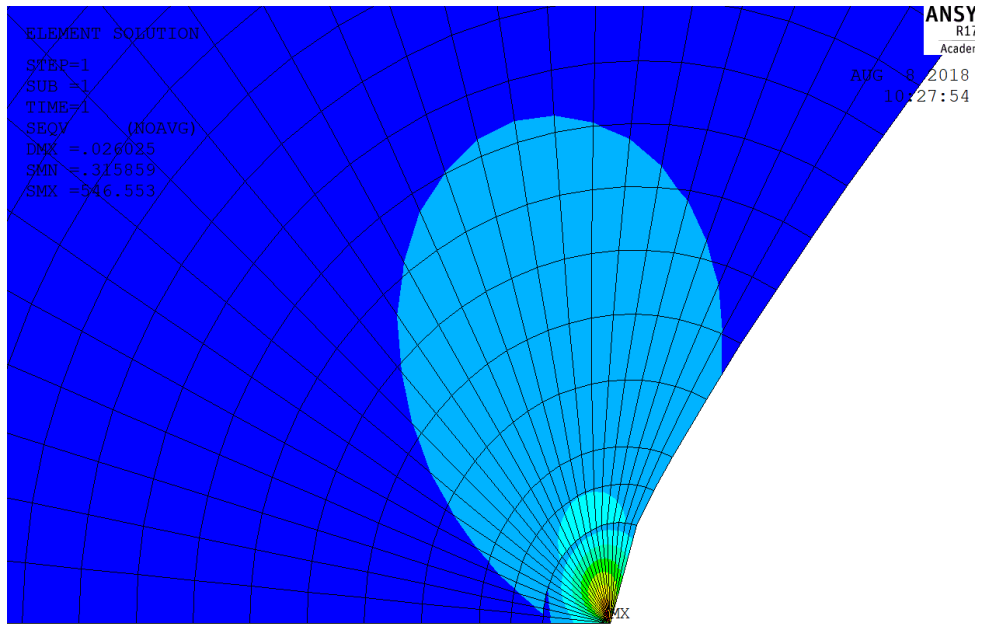


FIGURE 25 EQUIVALENT STRESS IN THE ELASTIC AND PLASTIC MODEL (40 MPA)

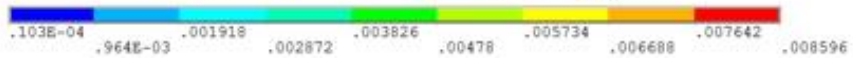
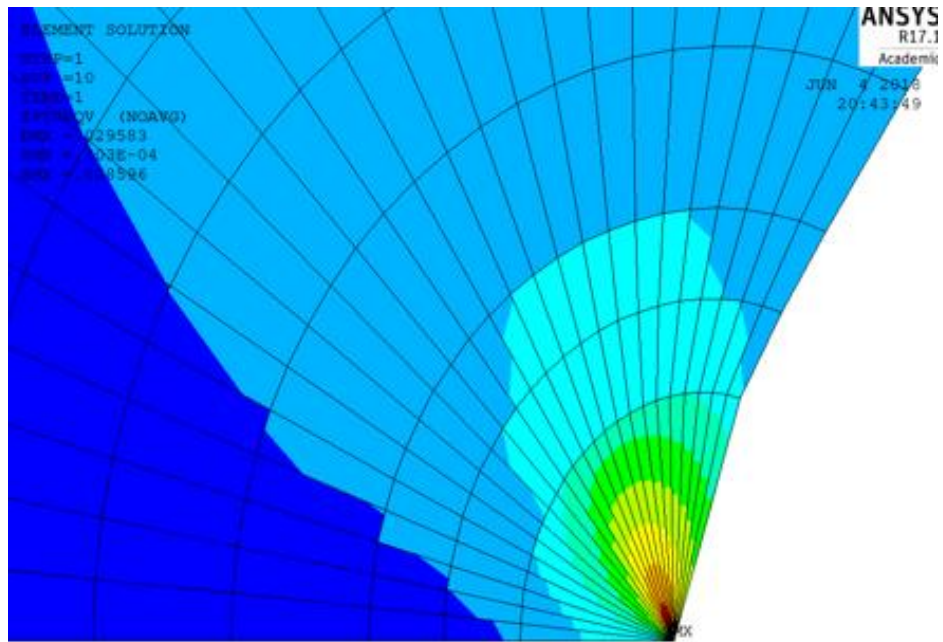
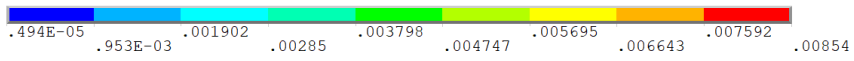
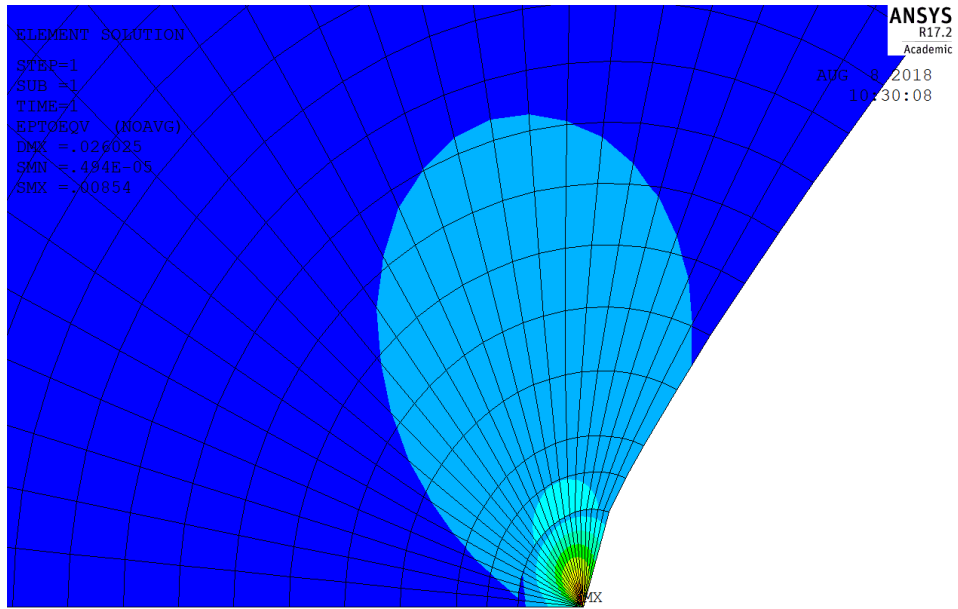


FIGURE 26 EQUIVALENT STRAIN IN THE ELASTIC AND PLASTIC MODEL (40 MPa)

If the load is high the difference of SED between the elastic and the plastic model is higher because the plastic region is bigger, in fact, for the highest load at which the specimens are loaded the difference is the 28%, which is anyway an acceptable error for the model used, while when the specimen is less loaded the difference is even less.

Stress [MPa]	Sene [Nmm]	Volu [mm3]	$W_{pl}$ [Nmm/mm3]	$W_{el}$ [Nmm/mm3]	error
120	0,035	0,017	2,038	1,465	28 %
40	0,003	0,017	0,186	0,163	12 %

The following plot is an output of Ansys and shows how the stress increases in time in the plastic model in a node close to the notch tip when the load is 120 MPa. It can be plotted using Time Hist Postpro, between the first and the second circumference closest to the notch tip with the finest mesh possible using the command kskon. It is clear that with a plastic model, the material yield and the stress reaches a plateau at 315 MPa.

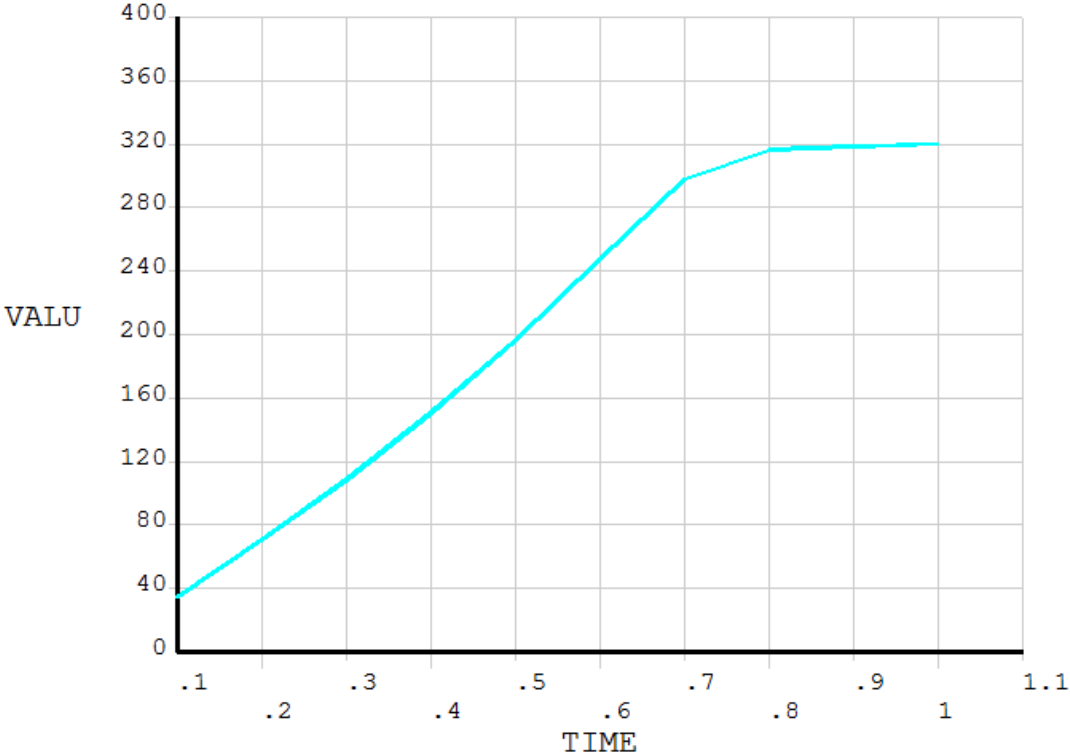


FIGURE 27 STRESS VS TIME IN A NODE CLOSE TO THE NOTCH TIP

Time is equal to one when all the sub steps are completed. A convergence study is made to choose the correct number of sub steps. For a load of 40 MPa 10 of them are enough as shown in the plot below

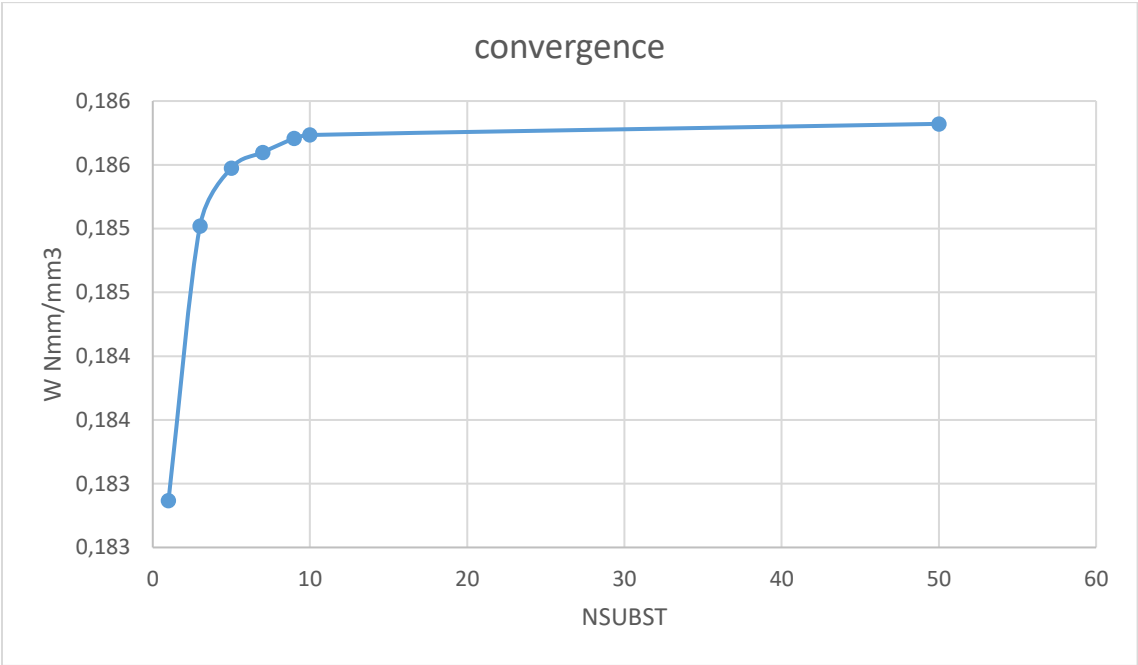


FIGURE 28 CONVERGENCE STUDY

10 subset are thus chosen for all the computations.

## 4. Computation of the Notch Stress Intensity Factor

As explained in the initial review the N-SIF cannot be used to draw the Wöhler curve when the geometry changes because its unit depends on an exponent which varies with the V-notch angle.

This problem has been overcome by using the mean value of the strain energy density range present in a control volume of radius  $R_c$  surrounding the area near the stress concentration.

Once SED is known, the N-SIF can though be calculated, through the following expression (9):

$$K_1^N = (R^*)^{1-\lambda_1} \sqrt{\frac{E \bar{W}}{e_1}} \quad (4.1)$$

$R^*$  has here been assumed to be equal to  $R_0$ , the critical radius of the material.

The values of  $\lambda_1$  and  $e_1$  for an opening angle of  $90^\circ$  can be found in literature

The notch stress intensity factor has been computed both using SED and stresses and the results are compared, showing that SED method is very precise even though less elements are required in the FEM model.

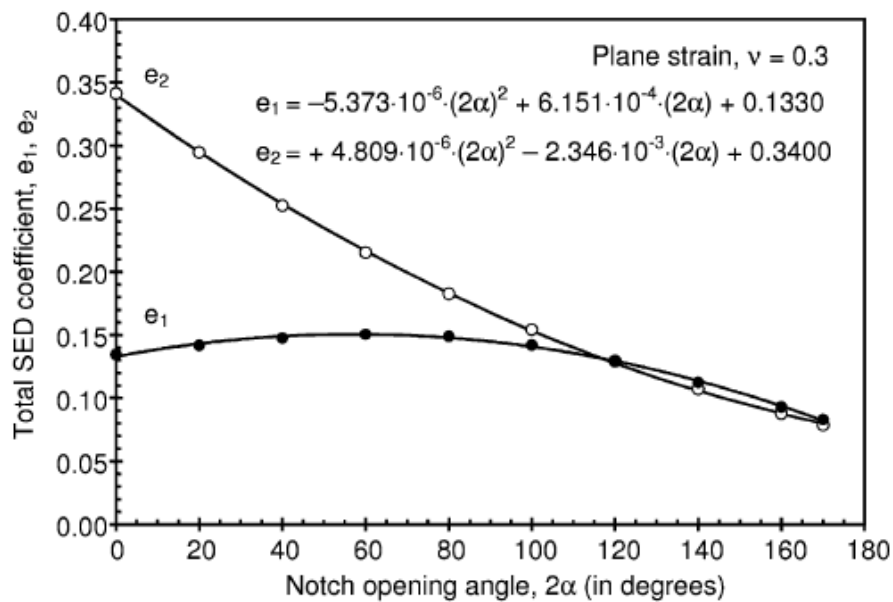


FIGURE 29 SHAPE FUNCTIONS  $e_1$  AND  $e_2$  VERSUS THE NOTCH OPENING ANGLE (9)

$2\alpha$ (rad/ $\pi$ )	$q$	$r_0/\rho$	Mode I			Mode II		
			$\lambda_1$	$\chi_1$	$\mu_1$	$\lambda_2$	$\chi_2$	$\mu_2$
0	2.000	0.500	0.500	1.000	-0.500	0.500	1.000	-0.500
1/6	1.833	0.455	0.501	1.071	-0.424	0.598	0.921	-0.259
1/4	1.750	0.429	0.505	1.166	-0.389	0.660	0.814	-0.145
1/3	1.667	0.400	0.512	1.312	-0.354	0.731	0.658	-0.033
1/2	1.500	0.333	0.544	1.841	-0.280	0.909	0.219	0.190
3/4	1.250	0.200	0.674	4.153	-0.150	1.302	-0.569	0.553

It is possible to compute  $K_I$  with the following expression, using stresses (9)

$$K_I = \lim_{r \rightarrow 0} \sqrt{2\pi r} \sigma \quad (4.2)$$

In which  $r$  is the distance from the notched tip and  $\sigma$  is the stress applied.

As it was expected the stress rise to a singularity at the pointed crack tip, while, in a radius close to the notch tip, the N-SIFs calculated express a plateau, which is a good estimate of the N-SIFs.

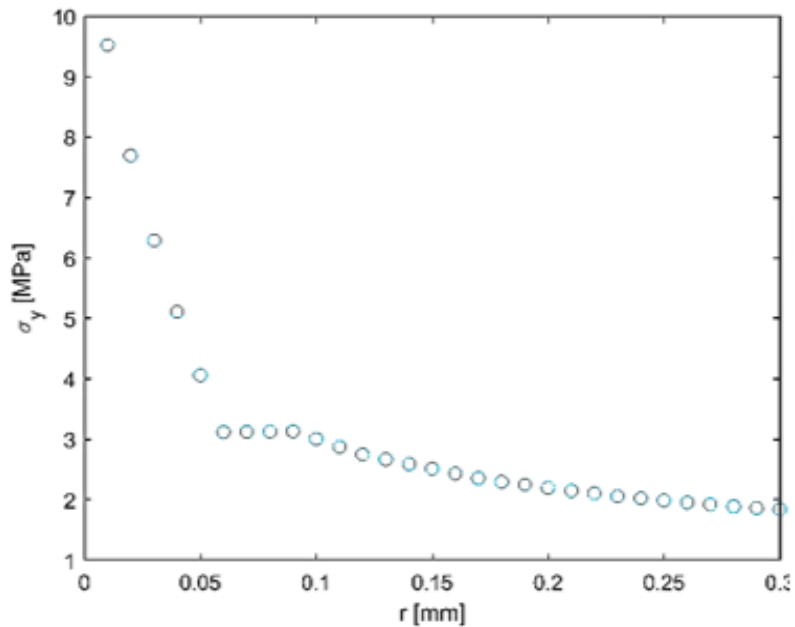


FIGURE 30 PLOT OF STRESS IN FUNCTION OF THE DISTANCE FROM THE TIP



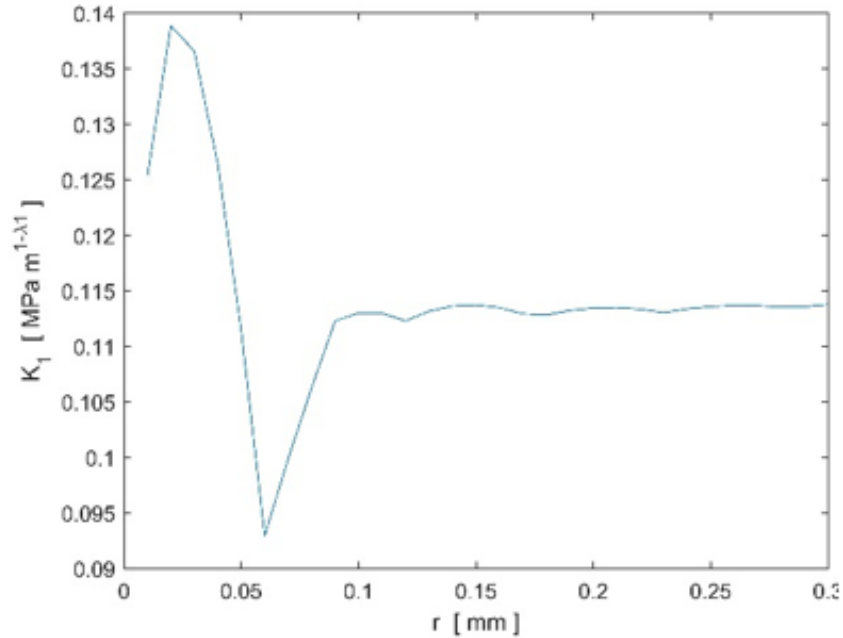


FIGURE 31 PLOT OF NSIF IN FUNCTION OF THE DISTANCE FROM THE TIP

Stresses obtained at a node belonging to faced finite elements are very different when a coarse mesh is used. As a natural consequence, the degree of mesh refinement required for the accurate determination of the strain energy is much lower than that required for the stress fields, simply because in the former case no derivation or integration process is really involved (11).

In fact, the mesh used to compute  $K_1$  through stresses is more refined than the one used with SED, as shown in the following figure

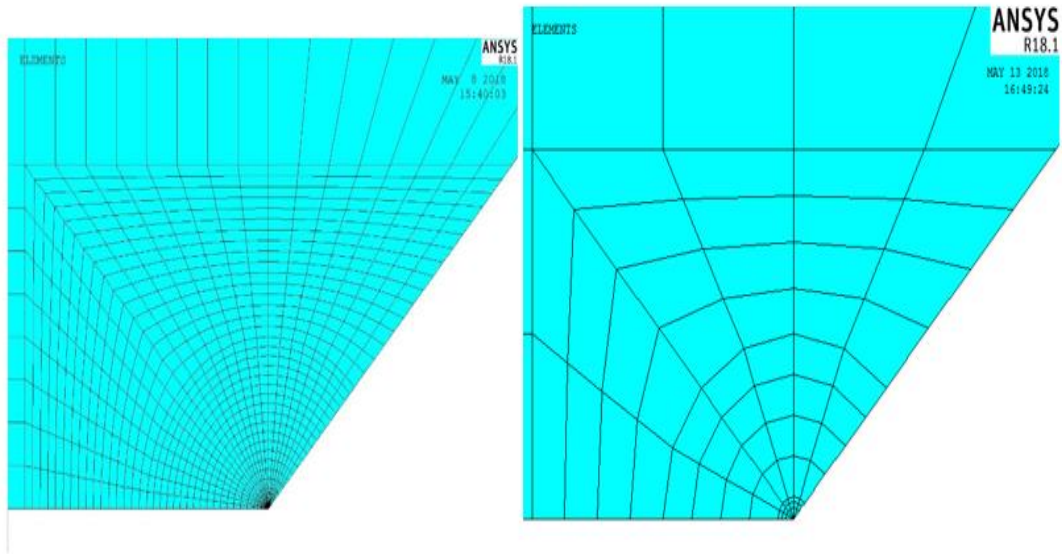


FIGURE 32 COMPARISON BETWEEN REFINE AND COARSE MESH

The values of  $K_1$  computed are very similar as it is shown in the table below

$K_1$ [MPa mm <sup>1-λ<sub>1</sub></sup> ]		
stress	SED	difference
0,113	0,109	3,6%

A comparison between plane strain and plane stress has been made to verify that the value of  $K_1$  is lower in conditions of plane stress.

$K_1$ [MPa mm <sup>1-λ<sub>1</sub></sup> ]		
Plane Stress	Plane Strain	difference
0,101	0,111	9,5%

A comparison has been made by plotting the scatter curve for the welded aluminum and the values of SED calculated for the samples tested.

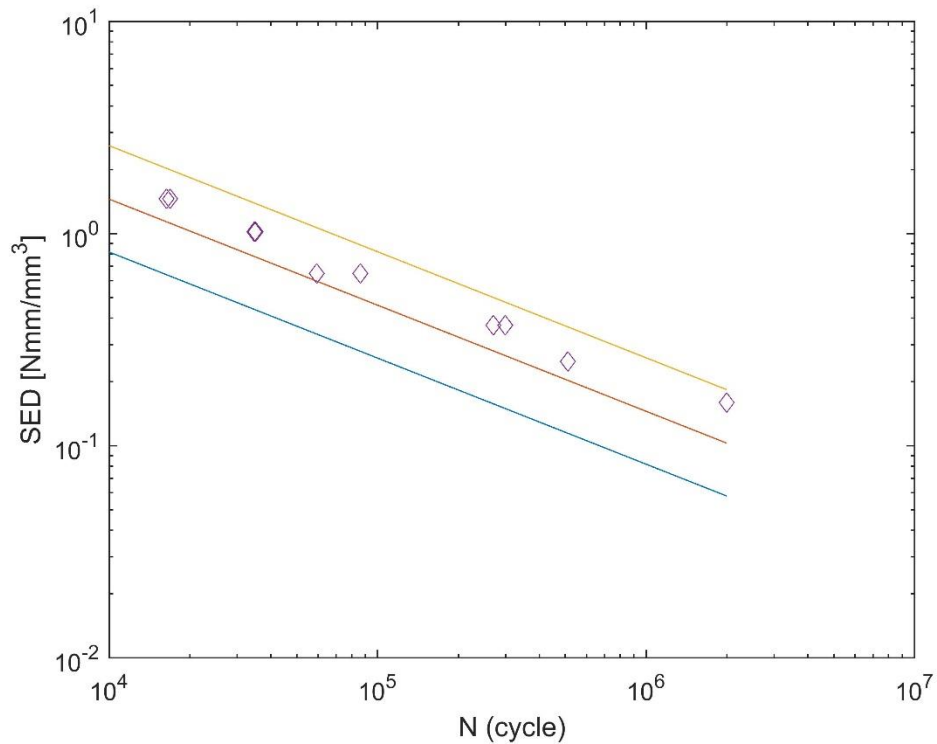


FIGURE 33 DATA FITTING IN WELDED ALUMINUM SCATTER BAND

As expected, the values computed for the samples fit in the welded aluminum scatter curve and they seem to be more resistant than the welded specimens.

## 5. Dimensionless Parameter Y

The stress intensity factor can be defined as

$$\Delta K = \sigma Y \sqrt{a} \quad (5.1)$$

In which  $\sigma$  is the stress applied,  $a$  is the length of the crack and Y is a dimensionless parameter.

Using a parametric Ansys model and the expression above it is possible to compute the value of Y, while the crack is progressing.

The aim is to find an expression for Y, suitable for V-shape notches, with an opening angle of  $90^\circ$ , in function of the ratio between the crack's length and the width of the sample.

When the SED is known it is possible to calculate  $K_1$  by the well-known expression

$$K_1 = R_0^{1-\lambda_1} \sqrt{\frac{EW}{e_1}} \quad (5.2)$$

In which  $\lambda_1$  and  $e_1$  must be computed for an angle of  $0^\circ$

A fourth-grade polynomial can fit the values obtained

$$Y\left(\frac{a}{W}\right) = 5852\left(\frac{a}{W}\right)^4 - 7647\left(\frac{a}{W}\right)^3 + 3712\left(\frac{a}{W}\right)^2 - 788.5\left(\frac{a}{W}\right) + 63.67 \quad (5.3)$$

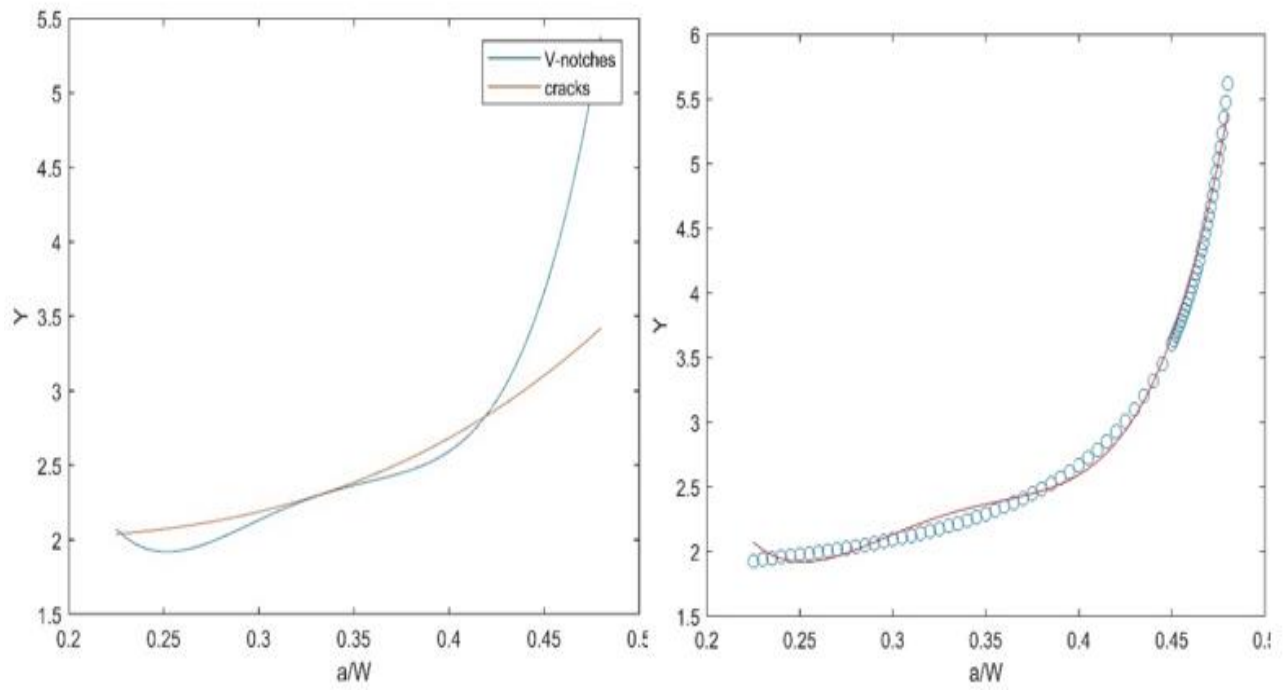


FIGURE 34 COMPARISON BETWEEN V-NOTCH AND CRACK AND DATA FITTING FOR V-NOTCH

This expression seems to be quite close to that used for double crack for low value of  $a$ , while the two curves tend to spread for high value of the crack's length.

## 6. Initiation and Propagation of the Crack

It is known from the paper written by Paris and Erdogan in 1963 (13) that by plotting on a log-log diagram the value of the derivative of the crack length with respect to of the number of cycles in function of the SIF, the data can be quite well fitted by a straight line, so the following expression can be written

$$\frac{da}{dN} = C\Delta K^n \quad (6.1)$$

Where C and n are two parameters which depend on the material and the load ratio.

The aim of this paper is to find a value of the coefficient C and n of the Paris' law, adapted for the Strain Energy Density.

$$\frac{da}{dN} = C'\Delta W^{n'} \quad (6.2)$$

In the case of non-singular mode II and considering a null opening angle of the notch it is possible to determine the mode I N-SIF a posteriori from SED, through the following expression

$$K_I = \sqrt{\frac{R_0 E W}{e_1}} \quad (6.3)$$

After some easy computation the parameters of interest and the number of cycles can be expressed in the following way

$$C' = C \left( \frac{R_0 E}{e_1} \right)^{n/2} \quad (6.4)$$

$$n' = n/2 \quad (6.5)$$

$$N_p = \int_{a_0}^{a_f} \frac{da}{C' W^{n'}} \quad (6.6)$$

W is a function of the length of the crack and can be found by fitting the different value of W while the crack is propagating. It is possible to compute an Ansys parametric model in which the stress at the restricted area  $\sigma_1$  is equal to 1 MPa and find the function  $W_1(a)$ , expressed by an exponential function

$$W_1(a) = A \exp(B a) + C \exp(D a) \tag{6.7}$$

In which  $A = 3.223E - 5$ ;  $B = 0.2868$ ;  $C = 1.858E - 14$ ;  $D = 2.608$

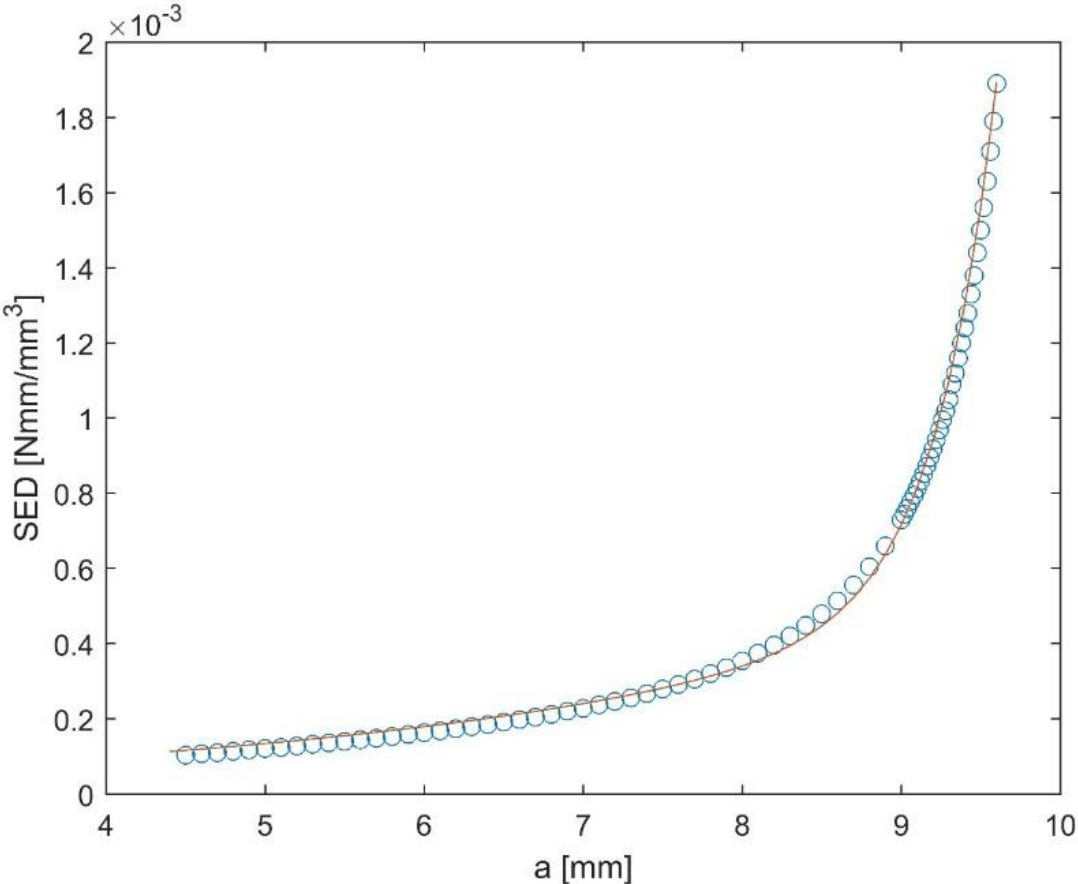


FIGURE 35 SED IN FUNCTION OF THE LENGTH OF THE CRACK

To find the function  $W(a)$  for each specimen the following expression can be used

$$W(a) = W_1(a) \cdot \sigma^2 \tag{6.8}$$

In which  $\sigma$  is the value of stress at the restricted area.

Finally, the number of cycles between the initiation of the crack and the failure of the specimen is

$$N_p = \frac{1}{C' \sigma^{2n'}} \int_{a_0}^{a_f} \frac{da}{W_1(a)^{n'}} \quad (6.9)$$

Where  $a_f$  has been measured from the crack surface.

The integral can be numerically solved using the '*integral*' function in matlab and considering that the value of the Paris' parameters for the aluminum alloy 6082-T6 are present in literature (16). Also the number of cycles necessary to initiate the crack can be computed

$$C' = 6.1154e - 05 \quad (6.10)$$

$$n' = 1.3235 \quad (6.11)$$

$$N_i = N_f - N_p \quad (6.12)$$

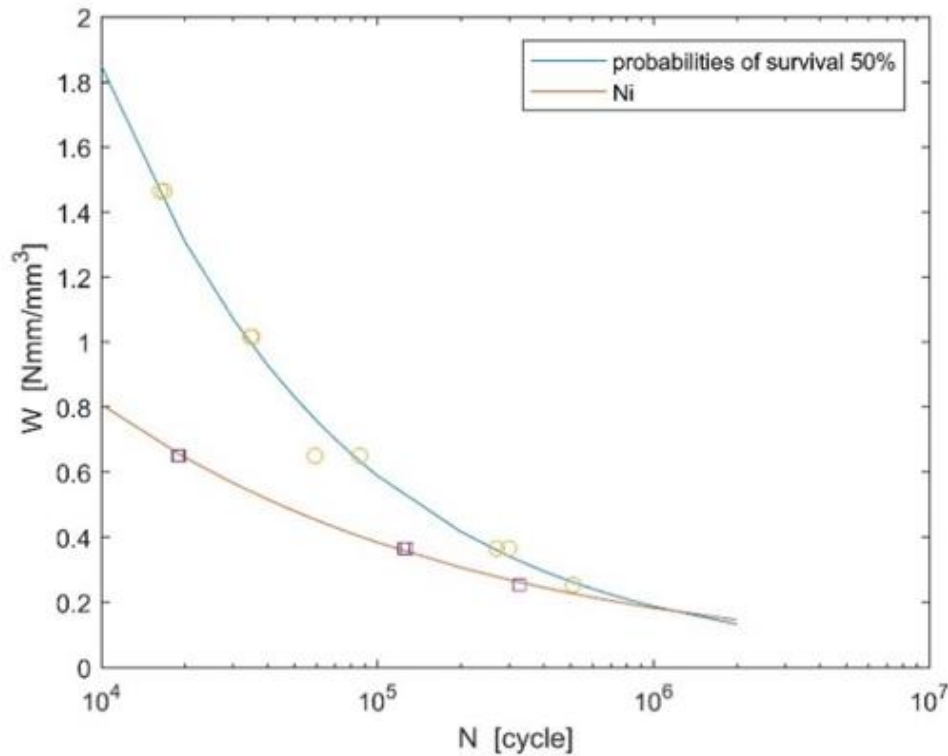


FIGURE 36 SED IN FUNCTION OF THE NUMBER OF CYCLES IN SEMI-LOG PLOT



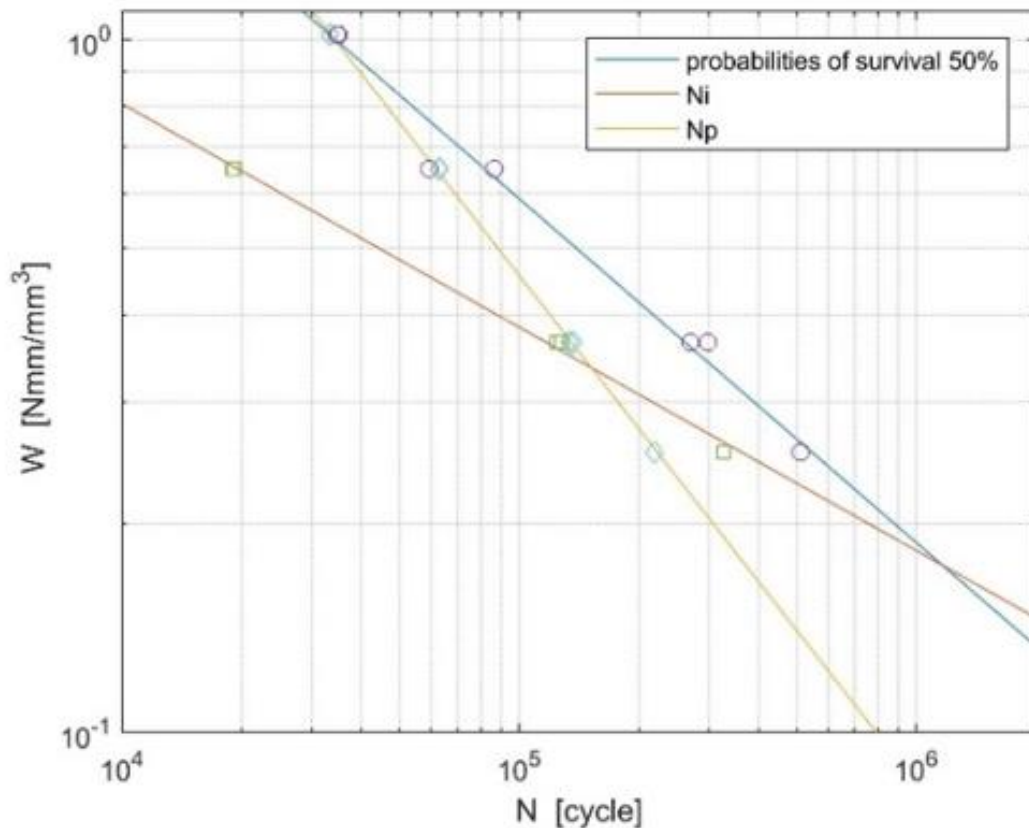


FIGURE 37 SED IN FUNCTION OF THE NUMBER OF CYCLES IN LOG-LOG PLOT

From the figures it is clear that at low cycles the propagation is prevalent, while at high cycle the initiation is so. For very low cycle the  $N_p$  exceeded the whole life of the specimen and this is clearly a mistake due to the approximations made. This model gives good result in a range between  $3 \cdot E04$  and  $1 \cdot E06$  cycles and outside this range the  $N_p$ , computed using the Paris' law is different from its actual value. Another relevant observation is that the shift from a life of the specimen dominated by the propagation of the crack to that dominated by the initiation occurs between  $1 \cdot E05$  and  $2 \cdot E05$  cycles, this is due to the fact that the specimen has a sharp notch, so the crack initiates earlier than in an un-notched one.

No experiments were made to compute the parameters  $C$  and  $n$  and they are taken from literature, for this reason the focus of this chapter is the analytical part, useful to find equivalent parameters and to apply Paris law to SED, even though the results seems to be consistent.

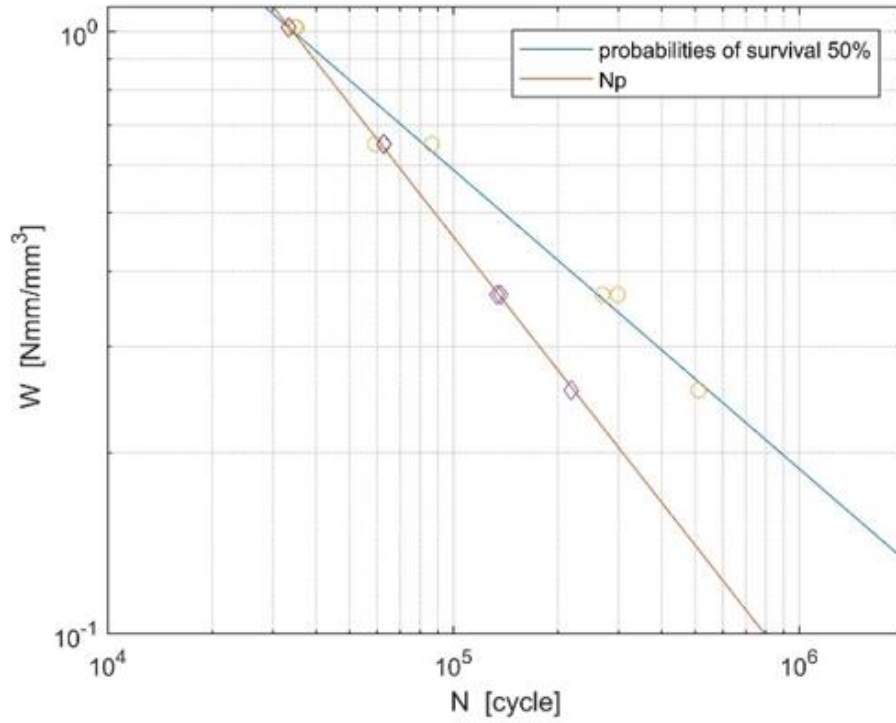


FIGURE 38 INFLUENCE OF SED ON THE PROPAGATION OF THE CRACK

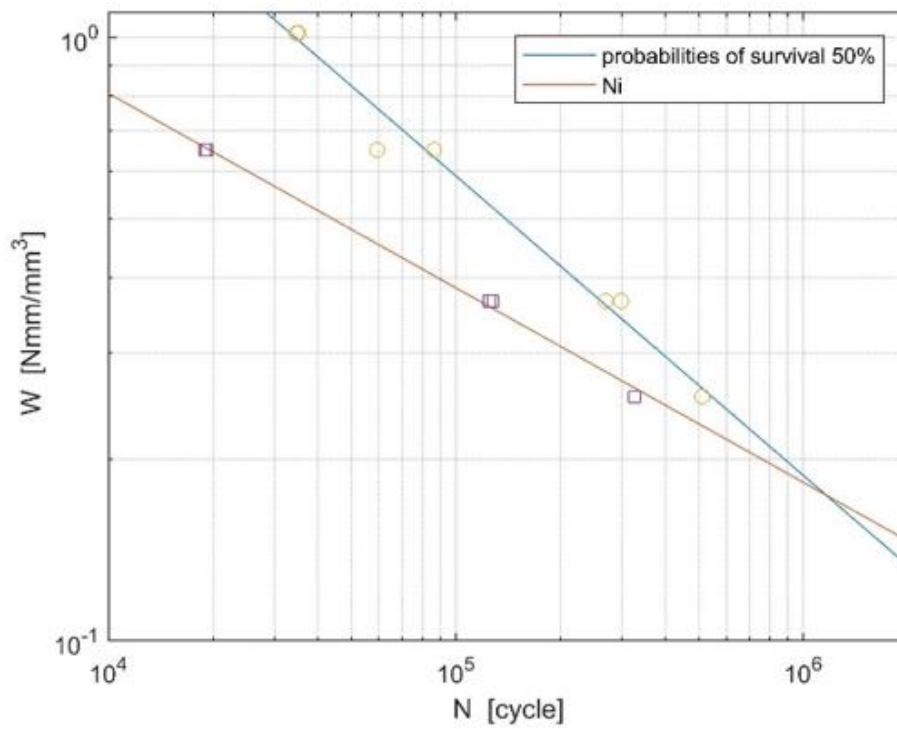


FIGURE 39 INFLUENCE OF SED ON THE INITIATION OF THE CRACK

## 7. Haigh Diagram

Both the data from the specimens loaded with  $R=0$  and  $R=0.5$  are used to plot the Haigh diagram using SED formulation. The coordinates of each point belonging to the plot are mean SED, alternative SED and number of cycles to failure. This plot has been projected on the  $W_m, W_a$  plane.

The SED components cannot be computed in a similar way to that used for the stress ones:

$$W_{max} = W_1 \cdot \sigma_{max}^2 \quad (7.1)$$

$$W_{min} = W_1 \cdot \sigma_{min}^2 \quad (7.2)$$

$$W_a = \frac{W_{max} - W_{min}}{2} \quad (7.3)$$

$$W_m = \frac{W_{max} + W_{min}}{2} \quad (7.4)$$

As explained in the Chapter dedicated to the Paris method, integrated with SED,  $W_1$  is the value of SED, when the specimen is loaded with a stress of  $1 \text{ MPa}$  at the restricted area.

Using these definitions both the Wöhler and Haigh plot are nonsense, because it seems that when the load ratio increases the material can resist to a higher  $W_a$  as it is shown in the following plot

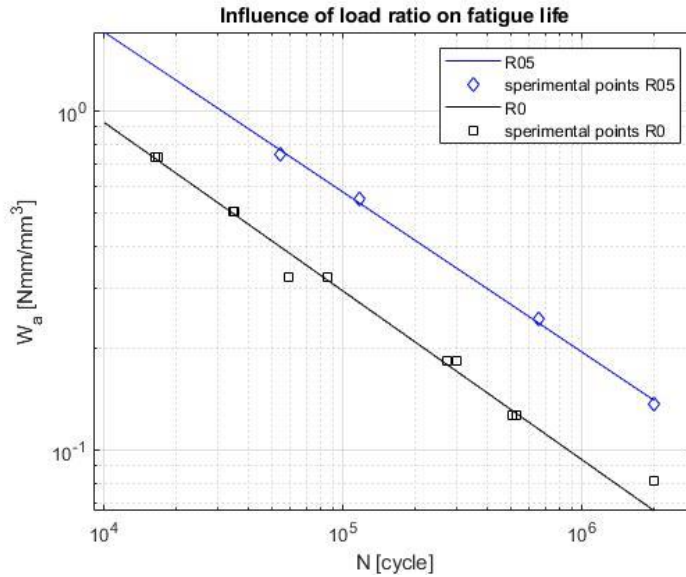


FIGURE 40 ERRONEOUS WÖHLER DIAGRAM

To avoid such problems, it is necessary to define new variables which are not the actual values of the mean and alternative components of SED, but allows to plot a meaningful Haigh plot:

$$W'_m = W_1 \sigma_m^2 \quad (7.5)$$

$$W'_a = W_1 \sigma_a^2 \quad (7.6)$$

Knowing that:

$$\sigma_a = \frac{\sigma_{max} - \sigma_{min}}{2} \quad (7.7)$$

$$\sigma_m = \frac{\sigma_{max} + \sigma_{min}}{2} \quad (7.8)$$

Consequently for R=0.5

$$W'_m = 9 \cdot W'_a \quad (7.9)$$

It is now necessary to find a point correspondent to the  $\sigma_{uts}$  in the Haigh diagram plotted with SED, through which it is possible to draw the iso number of cycles lines, using the Gerber relation.

If  $K_{Ic}$  is known, this point can be easily found from the well-known formula that relates SED with the mode I of N-SIF:

$$W_u = \left( \frac{K_{Ic} e_1}{E R_0^{1-\lambda_1}} \right)^2 \quad (7.10)$$

In which the value of  $\lambda_1$  and  $e_1$  are those related to an opening angle of  $0^\circ$

Since  $K_{Ic}$  is not known,  $W_u$  is computed doing the mean of the value of SED at the fracturing point of all the specimen loaded with a null load ratio.

Knowing that the value of SED for a load of 1 MPa in function of the length of the crack is expressed by (6.7)

It is necessary to measure the length of the crack on the fractured surface to compute the value of SED. This procedure is made for all the samples loaded with  $R=0$  and the mean value of SED right before the rupture of the specimen is

$$W_u = 3.41 \text{ N} \cdot \text{mm}/\text{mm}^3 \quad (7.11)$$

specimen	af[mm]	W1(af) [Nmm/mm3]	Wf [Nmm/mm3]
2	8,08	3,53E-04	5,09
11	7,92	3,30E-04	4,75
6	8	3,70E-04	3,70
8	8,18	3,71E-04	3,71
3	8,78	5,63E-04	3,61
9	9	6,14E-04	3,93
5	8,68	5,15E-04	1,85
10	9,385	1,27E-03	4,56
16	8,63	4,94E-04	1,23
12	8,94	6,67E-04	1,67
			3,41

It can be noticed that the size of the final crack at fracture depends on the stress level. The higher stress levels have shorter critical crack sizes and the lower stress levels have larger critical crack sizes.

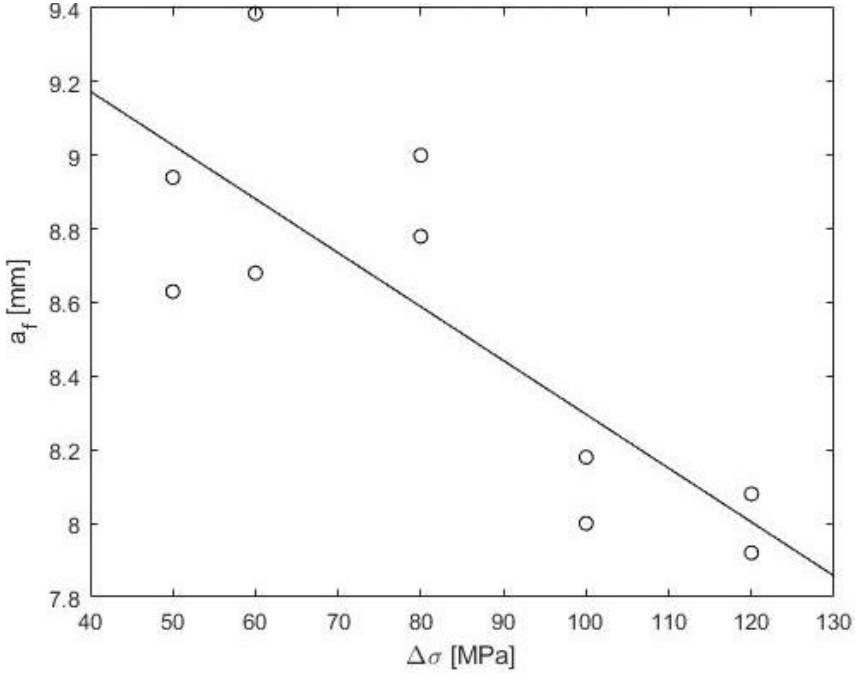


FIGURE 41 VARIABILITY OF THE FINAL LENGTH OF THE CRACK IN FUNCTION OF THE STRESS APPLIED FOR R=0

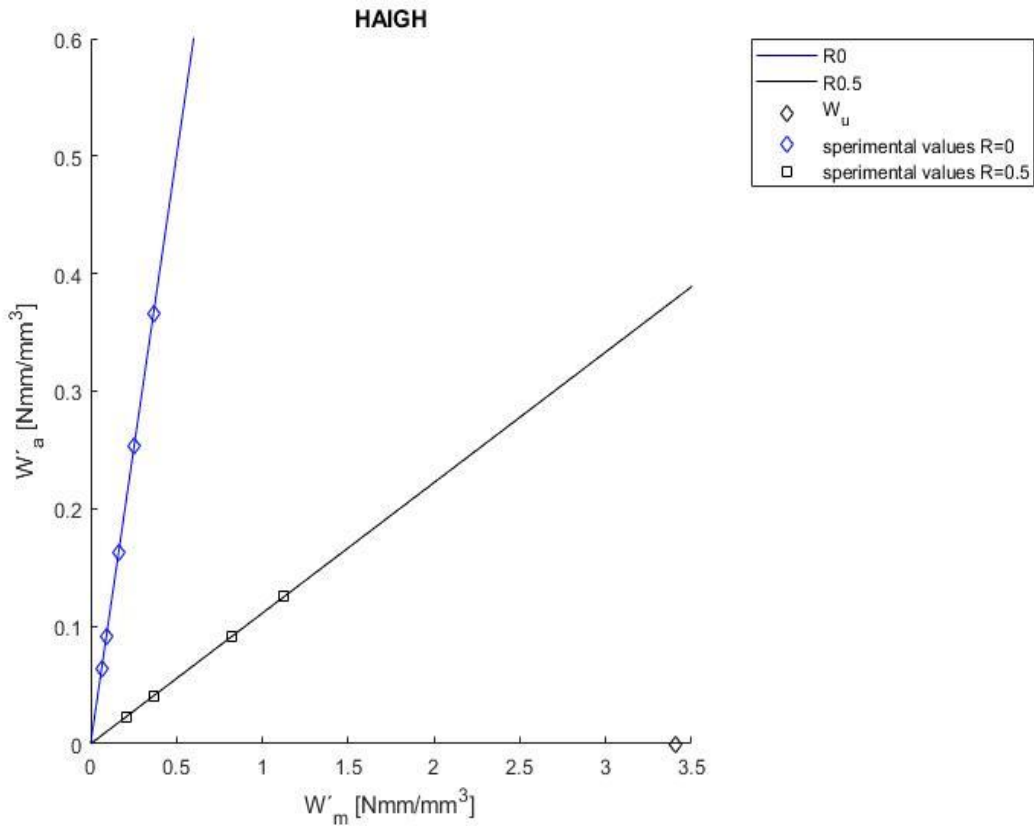


FIGURE 42 EXPERIMENTAL VALUES IN THE HAIGH DIAGRAM

In order to model the effect of the mean stresses, a multitude of formulations have been proposed, most of which use the engineering tensile stress  $\sigma_{uts}$  or the monotonic yield stress  $\sigma_y$  as one of the parameters.

In general, these formulas come from empirical approaches to correlate groups of tests on particular materials. In the literature it is widely documented that there is no general empirical law to relate the effect of mean stress on the fatigue limit (2).

The Gerber relation is used in the following diagrams, a parabola, concave downward that passes through the point  $W_u$  on the x-axis, interpolates the iso number of cycles point and crosses the y-axis with horizontal tangent.

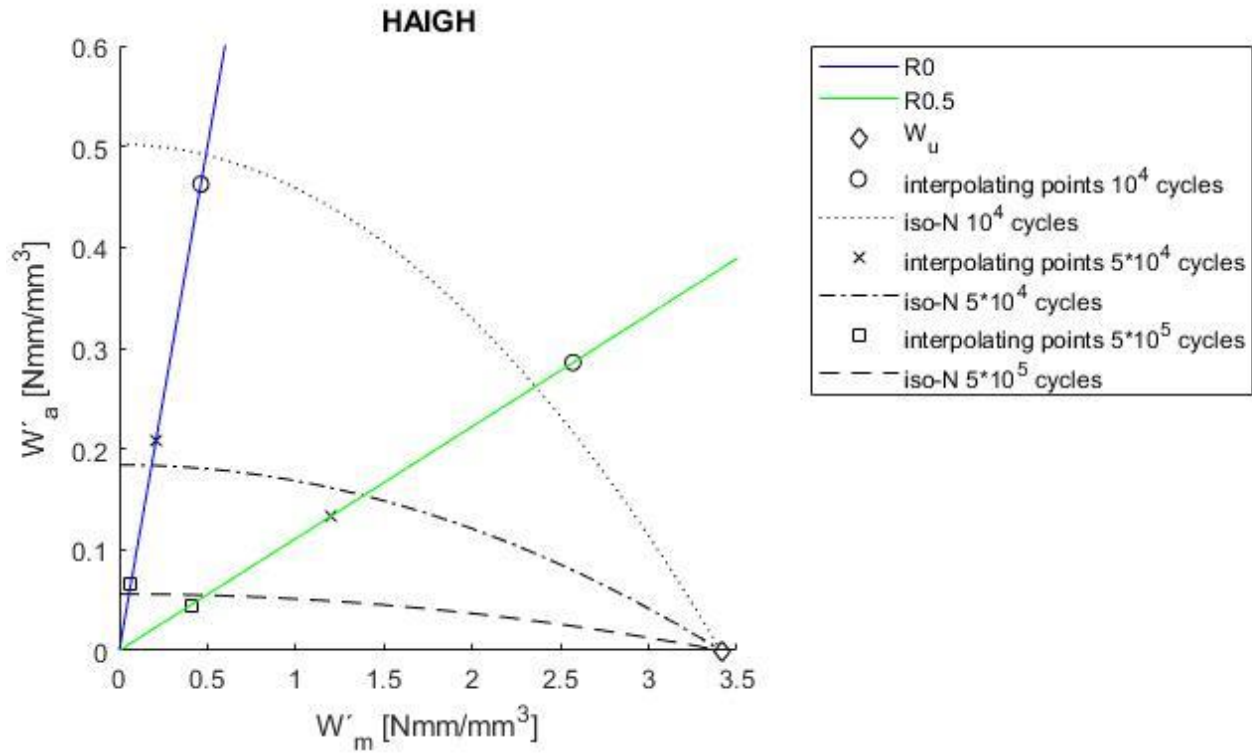


FIGURE 43 GERBER`S RELATION WITH SED

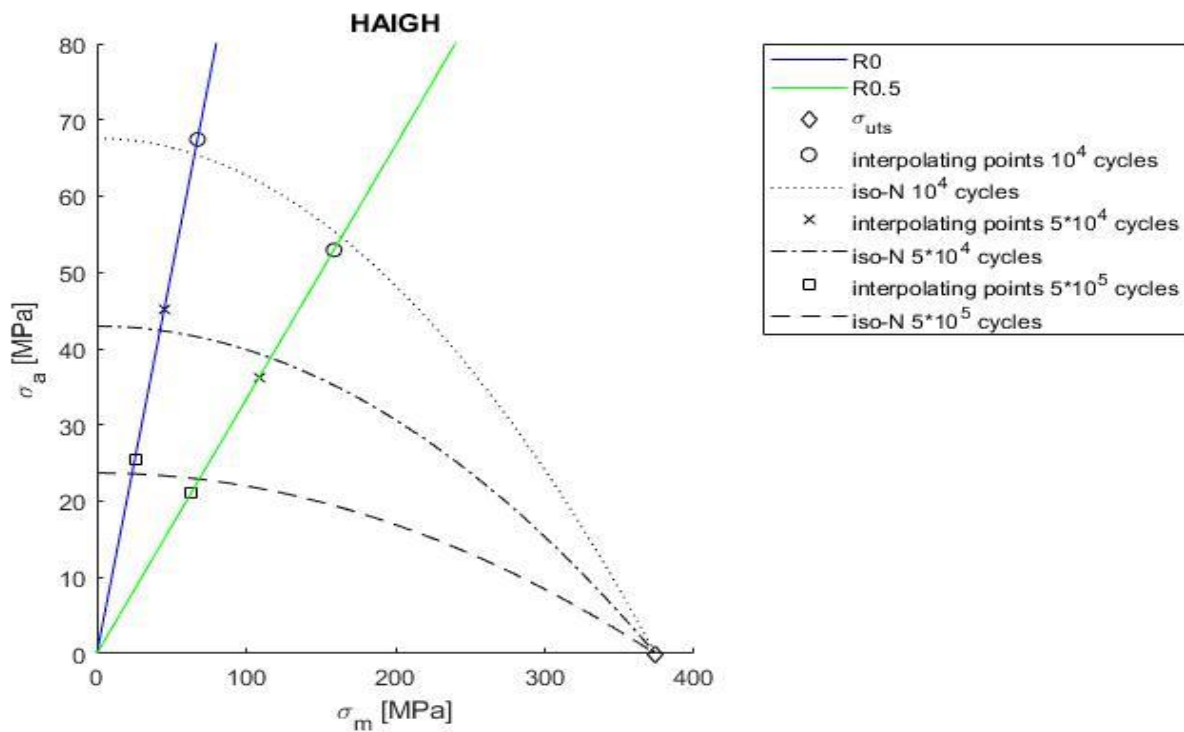


FIGURE 44 GERBER`S RELATION WITH STRESS



The number of cycles at the intersections between the Gerber parabola and the lines at R=0 and R=0.5 are graphically found and the ratio between the predicted life and the experimental one is computed:

Number of cycles computed with SED						
	R0			R0.5		
<b>Gerber</b>	1,0E+04	5,0E+04	5,0E+05	1,0E+04	5,0E+04	5,0E+05
<b>Experimental Life</b>	9,0E+03	6,5E+04	7,0E+05	1,2E+04	3,7E+04	3,3E+05
<b>Ratio</b>	1,1	0,8	0,7	0,8	1,4	1,5

Number of cycles computed with stress						
	R0			R0.5		
<b>Gerber</b>	1,0E+04	5,0E+04	5,0E+05	1,0E+04	5,0E+04	5,0E+05
<b>Experimental Life</b>	1,1E+04	6,5E+04	7,0E+05	9,0E+03	3,7E+04	3,5E+05
<b>Ratio</b>	0,9	0,8	0,7	1,1	1,4	1,4

The same procedure is adopted with the Goodman relation, represented in the diagrams by a line which passes through point  $W_{li}$  on the x-axis and interpolates the points underlined.

Number of cycles computed with SED						
	R0			R0.5		
<b>Goodman</b>	1,0E+04	5,0E+04	5,0E+05	1,0E+04	5,0E+04	5,0E+05
<b>Experimental Life</b>	8,6E+03	5,2E+04	6,0E+05	1,6E+04	4,7E+04	3,6E+05
<b>Ratio</b>	1,2	1,0	0,8	0,6	1,1	1,4

Number of cycles computed with stress						
	R0			R0.5		
<b>Goodman</b>	1,0E+04	5,0E+04	5,0E+05	1,0E+04	5,0E+04	5,0E+05
<b>Experimental Life</b>	9,0E+03	5,0E+04	5,6E+05	1,2E+04	5,0E+04	4,3E+05
<b>Ratio</b>	1,1	1,0	0,9	0,8	1,0	1,2

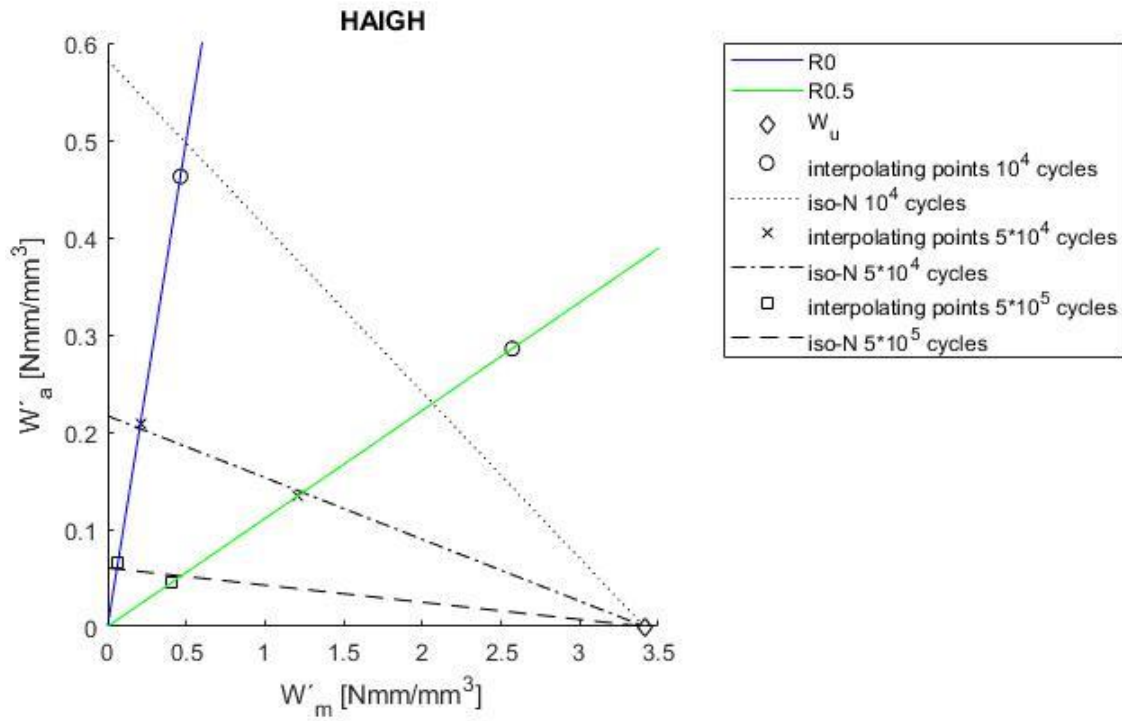


FIGURE 45 GOODMAN'S RELATION WITH SED

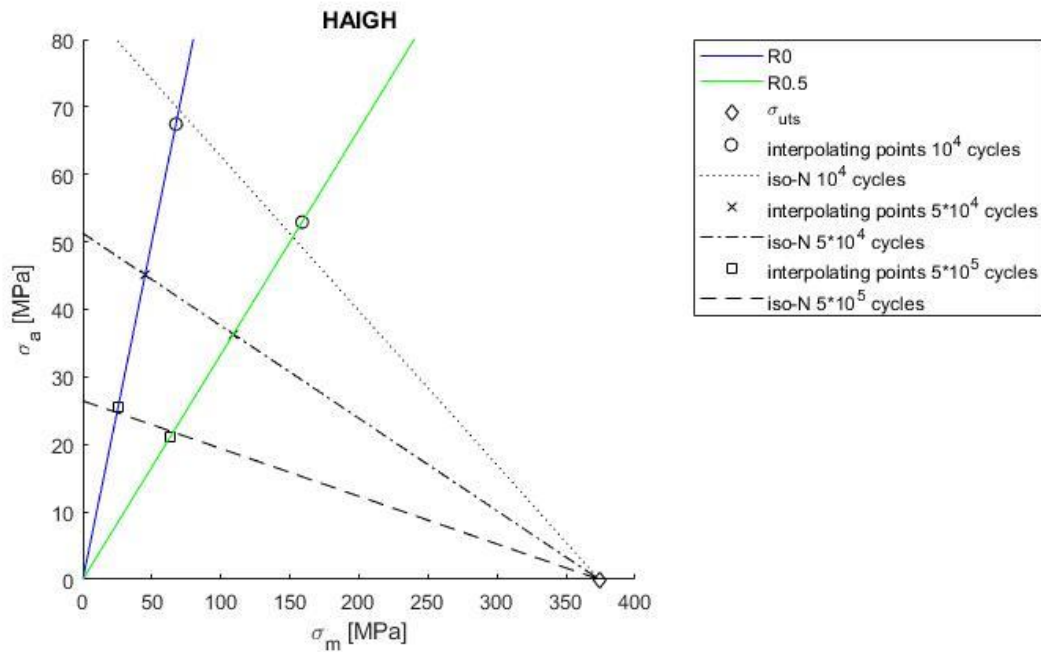


FIGURE 46 GOODMAN'S RELATION WITH STRESS

It is clear that using Gerber relation the precision is very similar using stress or SED, in both cases the critical point is that on the  $R=0.5$  line, because according to Gerber's relation the specimen should resist 50% and 40% more than it actually does, respectively in SED and stress's diagram. This level of precision is consistent with that present in the literature (17).

Goodman relation works better with the stress, even though the precision achieved with SED is also acceptable.

It is though possible to use SED method to plot the Haigh diagram, exploiting all the advantages linked to this method, especially for what concern the computation time and the possibility of using coarse meshes, as explained in the dedicated chapter.

## 8. Equivalent method to characterize the fatigue behavior of the aluminum specimen

The three parameters that characterize a mechanical fatigue behavior are the mean stress,  $\sigma_m$ , alternating stress,  $\sigma_a$  and the resulting life,  $N$ , the application of the data that characterize the mean and alternating stress in one equivalent stress model allows to evaluate their effect on the fatigue behavior.

The equivalent value of the stress use in this paragraph is calculated as the fatigue strength,  $\sigma_{-1}$ , when the load ratio  $R$  is equal to -1. For example in the Haigh diagram, the iso- $N$  curves, drawn using Goodman's relation, can be described by the following equation:

$$\sigma_a = \left( -\frac{\sigma_{-1}}{\sigma_{UTS}} \right) \sigma_m + \sigma_{-1} \quad (8.1)$$

Starting from the experimental data, alternative and mean stress are computed, after that the equivalent stress is calculated, both by using Goodman and Gerber models.

$$\sigma_{-1} = \sigma_{Go} = \frac{\sigma_a}{1 - \left( \frac{\sigma_m}{\sigma_{UTS}} \right)} \quad (8.2)$$

$$\sigma_{-1} = \sigma_{Ge} = \frac{\sigma_a}{1 - \left( \frac{\sigma_m}{\sigma_{UTS}} \right)^2} \quad (8.3)$$

The objective of this paragraph is to verify the possibility to apply this method, devised by the researchers of the Department of mechanical Engineering of the University of Brasília (18) to be used with stress, to SED.

All the data are fitted in the Wöhler plot and the R-squared value is computed using Matlab.

The method works well for the aluminum specimen, because both using Goodman and Gerber's relation, the value of R-squared increases.

The R-squared is a statistic value that gives some information about the goodness of fit of a model as explained in Appendix D and an  $R^2$  of 1 indicates that the regression predictions perfectly fit the data.

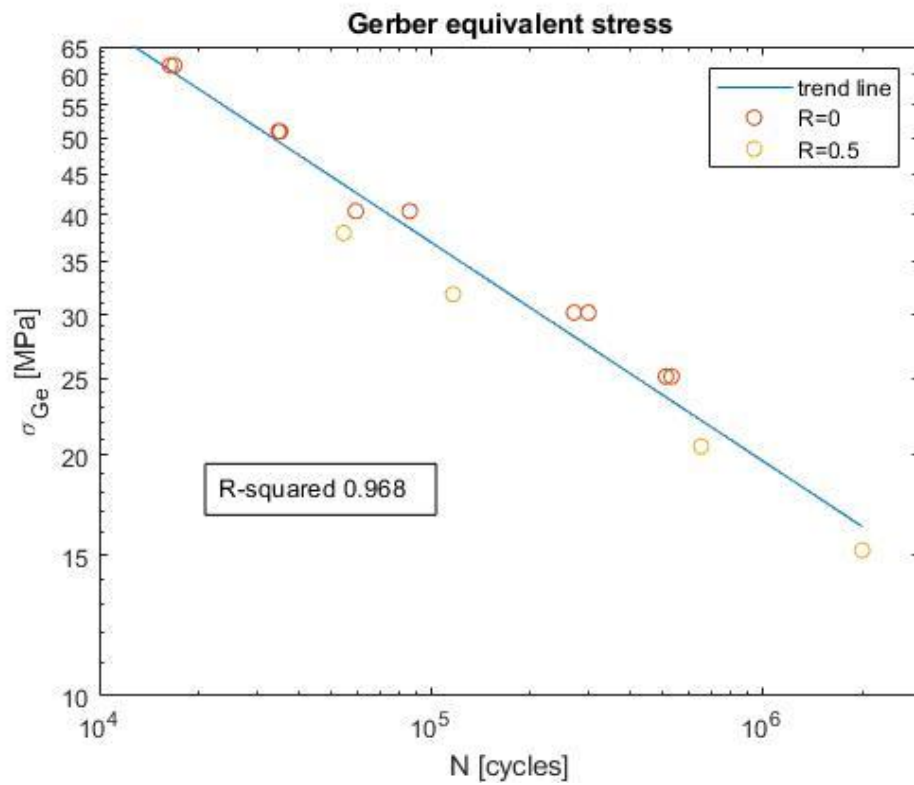
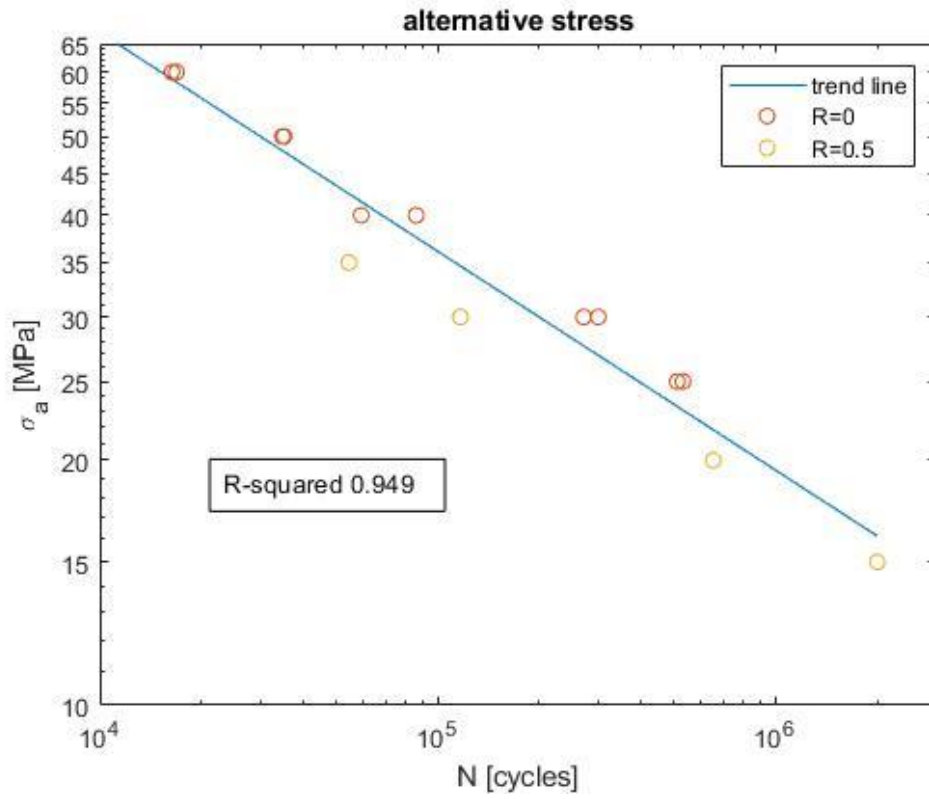


FIGURE 47 GERBER'S RELATION ON STRESS

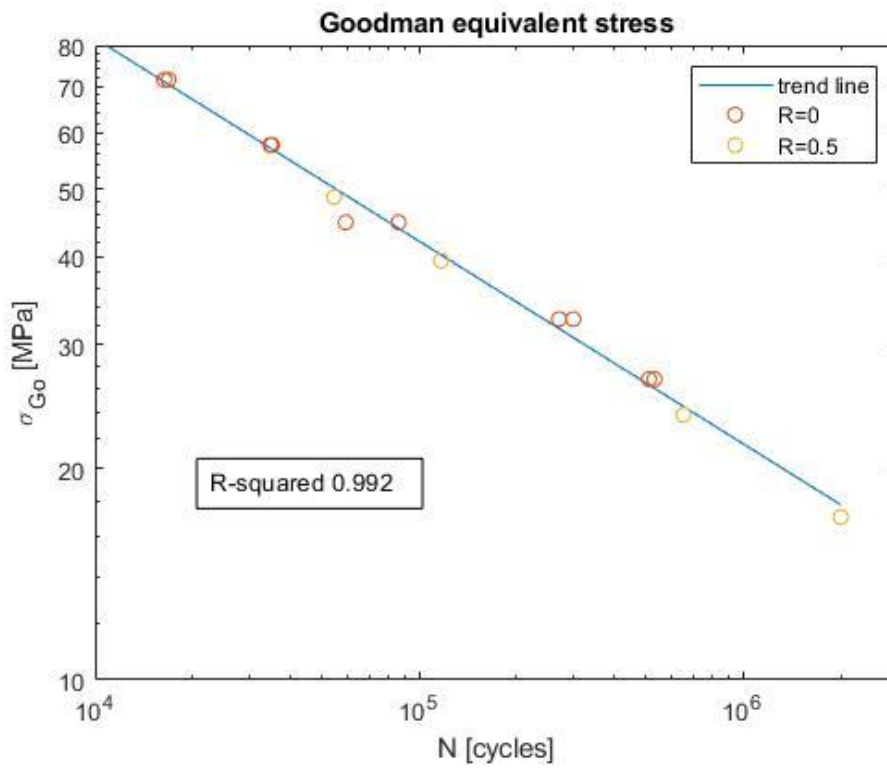
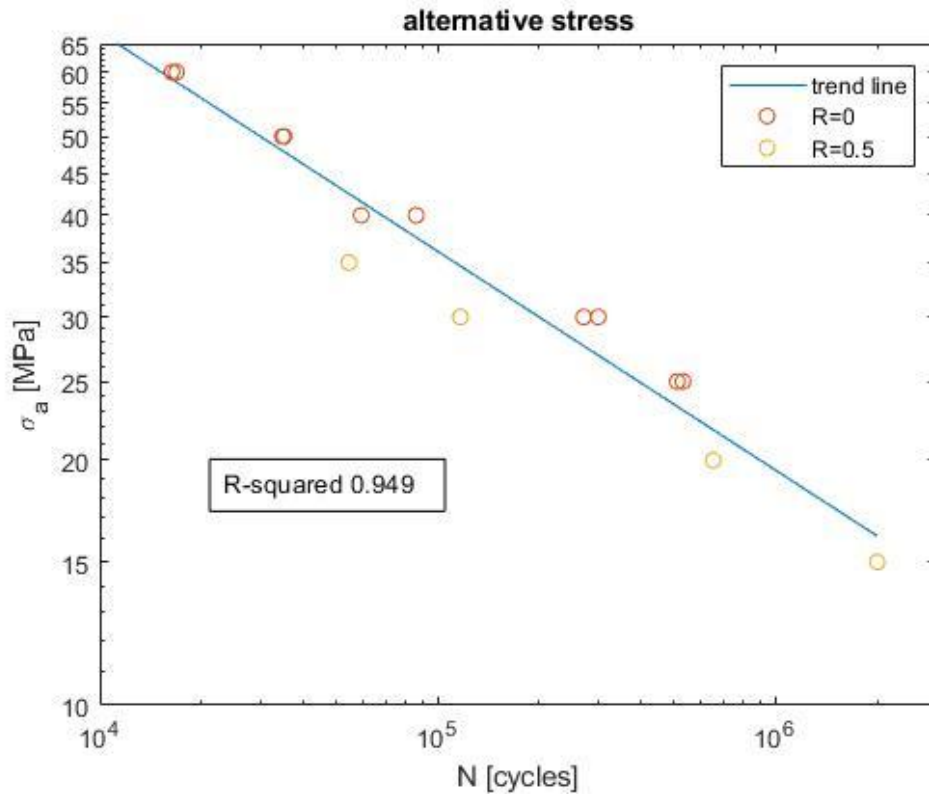


FIGURE 48 GOODMAN'S RELATION ON STRESS

The same variables ( (7.5) (7.6) and (7.11) ) defined to draw the Haigh plot are used in the following expressions and the Wöhler plot are again analyzed with SED:

$$\hat{W}_{a,Go} = \frac{\hat{W}_a}{1 - \left(\frac{\hat{W}_m}{\hat{W}_u}\right)} \quad (8.4)$$

$$\hat{W}_{a,Ge} = \frac{\hat{W}_a}{1 - \left(\frac{\hat{W}_m}{\hat{W}_u}\right)^2} \quad (8.5)$$

For both stress and SED there is a big advantage in using this method because in all cases the R-squared values sensibly increases, even though with SED this variance is bigger using Gerber method, while with stress is bigger using Goodman.

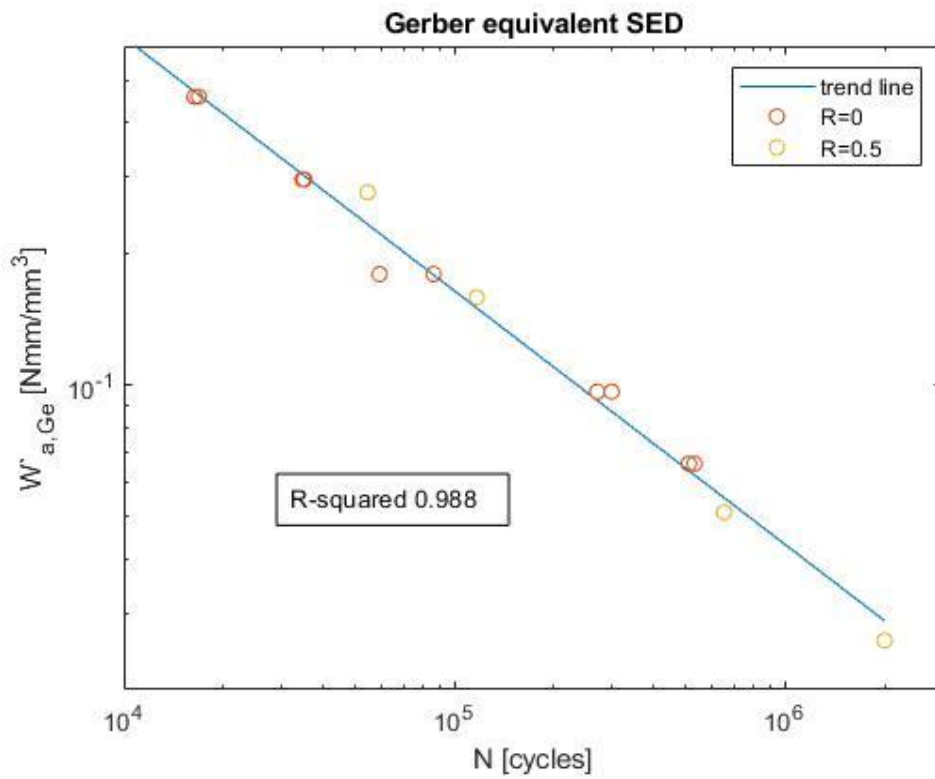
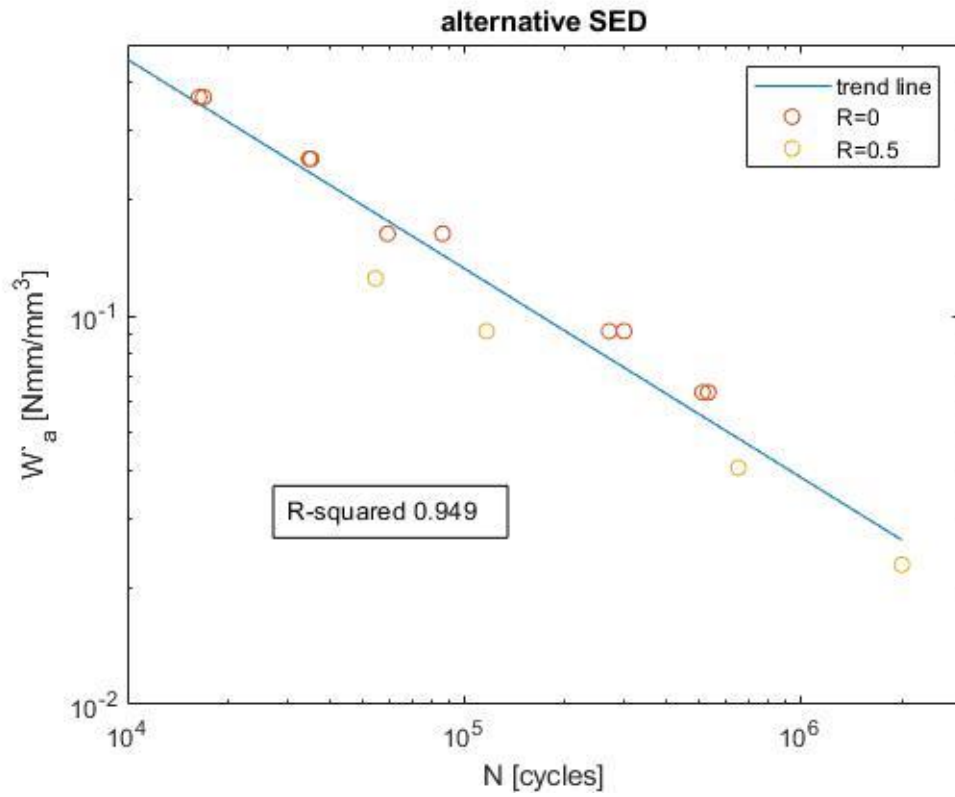


FIGURE 49 GERBER'S RELATION ON SED



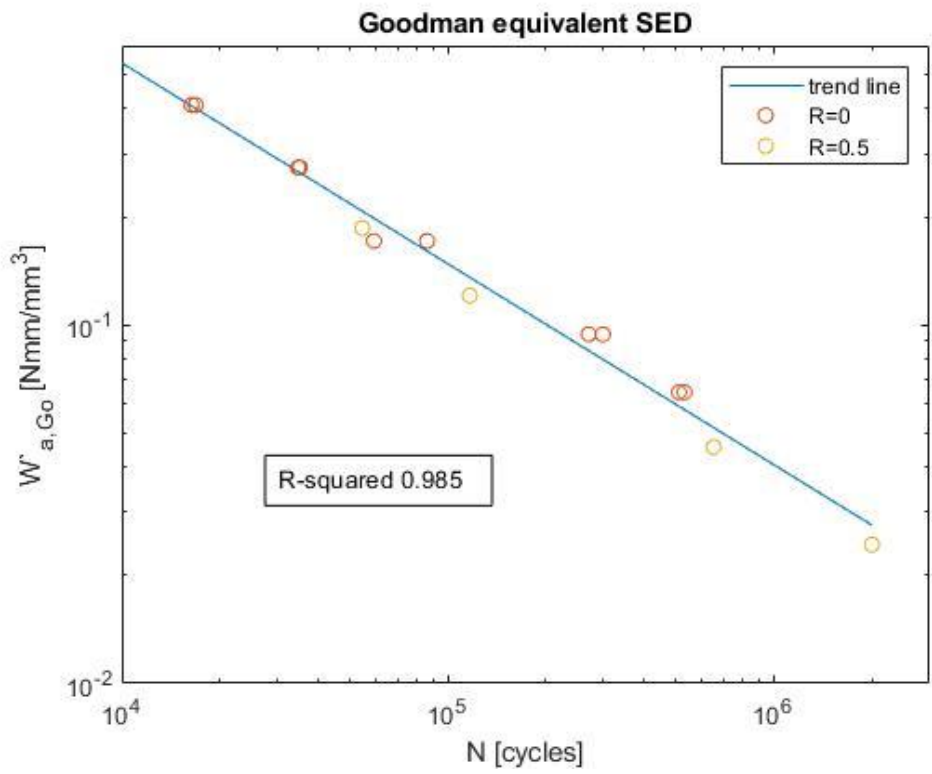
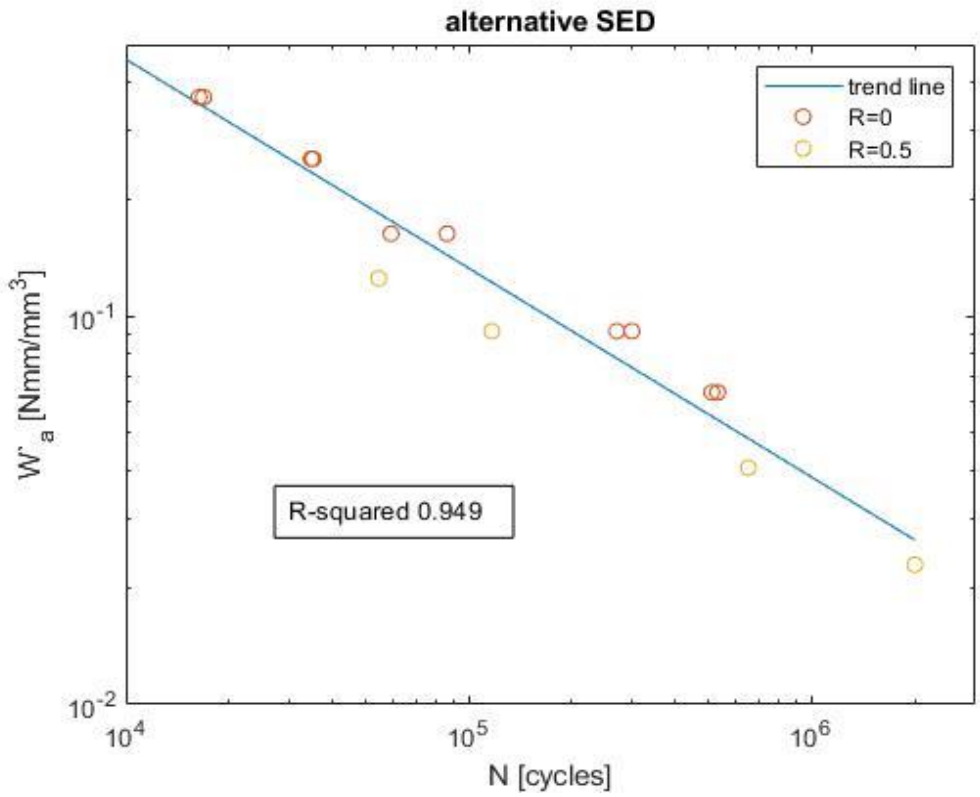


FIGURE 50 GOODMAN'S RELATION ON SED

## 9. Conclusion

SED method works well with the aluminum specimen and the value of the N-SIF is really close to that computed with stress, but a model with many less elements is sufficient. This is a great advantage, especially when complicated model are implemented and the computation time is much bigger than that needed for the sample, since its geometry is very simple.

For what concern the hypothesis and the simplifications adopted in this theory a particular focus on the difference between a plastic and elastic model is made.

The difference in the numerical values of SED can be quite high, and it depends a lot on the load applied to the specimen, because as it increases the region in which the material yields becomes bigger. In the plastic model the stress is limited but the strain increases and as a result the value of SED computed with this model is higher than that of the elastic one.

Anyway the method works well, as documented in the literature (8), (9), (11), and it is though possible to neglect the yield which occurs close to the notch tip, in a very restricted area. This hypothesis is very useful because it permits to use very simple models and less time consuming.

The theory works good in the Haigh diagram, in fact the precision is similar to that of the traditional Haigh diagram if the Gerber's relation is used. For this reason SED method can be applied and once the strain energy density is computed through FEM models the new Haigh diagram can be directly used.

A particular attention is necessary in considering the variables  $W'_m$  and  $W'_a$  used in the diagram not as the actual values of the mean and alternative component of the energy, but as two equivalent parameters defined to plot a meaningful Haigh plot, in which an increase of the load ratio leads to a reduction of the component's life. Another important parameter,  $W_u$ , is defined and the point  $(0; W_u)$  is the equivalent of the  $(0; \sigma_{uts})$  in the traditional Haigh diagram.

This method has also been extended to Paris theory, with the aim to predict the number of cycles necessary for the nucleation and propagation of the crack and to compute two equivalent parameters  $C'$  and  $n'$ , that can be used with SED. The analytical procedure is explained in detail in the dedicated chapter, but the parameters  $C$  and  $n$  of the Paris law are taken from the literature and not directly find through the experimental procedure, so the numerical results cannot be used for practical applications.

Finally it is demonstrated that also the equivalent method devised by Badibanga, Miranda et al. works well with SED if the same parameters,  $W_u$ ,  $W'_m$  and  $W'_a$ , defined for the Haigh diagram are used. Using the equivalent SED the dispersion of the experimental points from the

interpolating line decreases, as it happens for the stress. In the case of the samples tested the Goodman relation works better with the stress, while with SED the Gerber relation is slightly better.

## Appendix A

The three basic loading modes with singular stresses at the crack tip produce the following asymptotic stress distribution around the crack tip (7)

$$\sigma_{ij} = \frac{1}{\sqrt{2\pi r}} [K_I f_{I,ij}(\theta) + K_{II} f_{II,ij}(\theta) + K_{III} f_{III,kz}(\theta)] \quad (A.1)$$

(i, j = x, y and k = x, y or i, j = r,  $\theta$  and k = r,  $\theta$ )

The mode-related stress intensity factors (SIFs)  $K_I$ ,  $K_{II}$  and  $K_{III}$  depend on the magnitude of the load, the crack length and further geometrical parameters of the considered configuration.

The mode-related angle-dependent functions  $f_{I,ij}$ ,  $f_{II,ij}$  and  $f_{III,kz}$  describe the angular distribution of the stresses at the crack tip.

The equation above is strictly valid for  $r \rightarrow 0$  and approximately valid for values of  $r$  which are small in relation to the crack length and other geometrical parameters of the configuration.

These are the asymptotic stresses in the three singular loading modes, given in polar coordinates

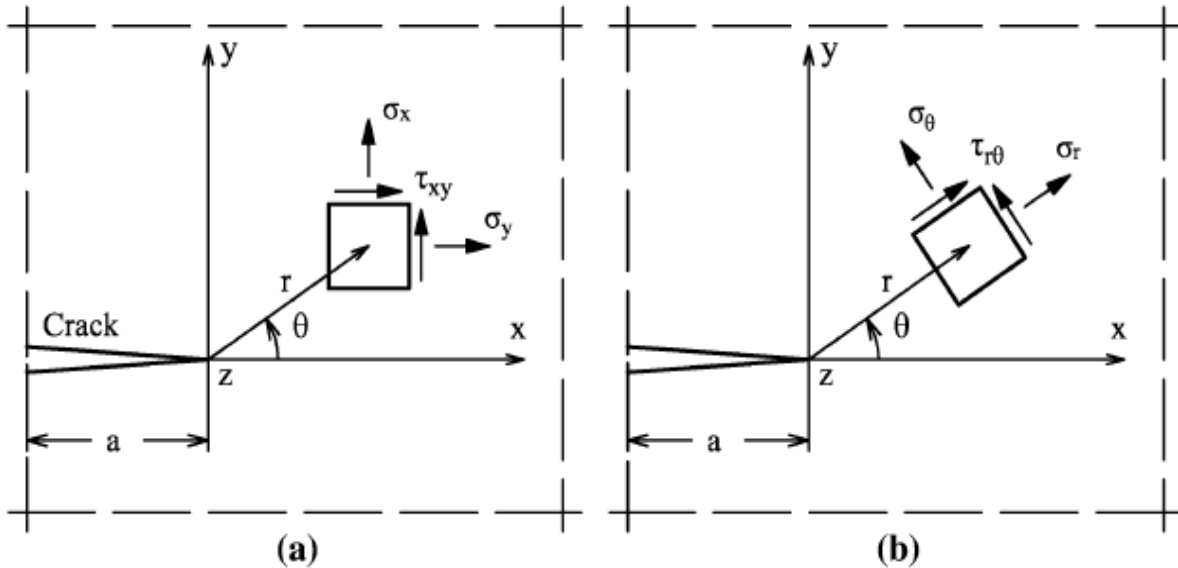


FIGURE 51 CARTESIAN (A) AND POLAR (B) COORDINATE SYSTEMS WITH STRESSES AT THE CRACK TIP (7)

Mode I

$$\begin{Bmatrix} \sigma_r \\ \sigma_\theta \\ \tau_{r\theta} \end{Bmatrix} = \frac{K_I}{4\sqrt{2\pi r}} \begin{Bmatrix} 5 \cos \theta/2 - \cos 3\theta/2 \\ 3 \cos \theta/2 + \cos 3\theta/2 \\ \sin \theta/2 + \sin 3\theta/2 \end{Bmatrix} \quad (A.2)$$

$\sigma_z = 0$  (plane stress)

$\sigma_z = \nu(\sigma_r + \sigma_\theta) = \frac{2\nu K_I}{\sqrt{2\pi r}} \cos \frac{\theta}{2}$  (plane strain)

Mode II

$$\begin{Bmatrix} \sigma_r \\ \sigma_\theta \\ \tau_{r\theta} \end{Bmatrix} = \frac{K_{II}}{4\sqrt{2\pi r}} \begin{Bmatrix} -5 \sin \theta/2 + 3 \sin 3\theta/2 \\ -3 \sin \theta/2 - 3 \sin 3\theta/2 \\ \cos \theta/2 + 3 \cos 3\theta/2 \end{Bmatrix} \quad (A.3)$$

$\sigma_z = 0$  (plane stress)

$\sigma_z = \nu(\sigma_r + \sigma_\theta) = -\frac{2\nu K_{II}}{\sqrt{2\pi r}} \sin \frac{\theta}{2}$  (plane strain)

Mode III

$$\begin{Bmatrix} \tau_{rz} \\ \tau_{\theta z} \end{Bmatrix} = \frac{K_{III}}{\sqrt{2\pi r}} \begin{Bmatrix} \sin \theta/2 \\ \cos \theta/2 \end{Bmatrix} \quad (A.4)$$

The SIFs  $K_I$ ,  $K_{II}$  and  $K_{III}$  may be determined from the following limit value formulae, which consider the predominant stresses in the ligament ( $\theta = 0$ ):

$$K_I = \lim_{r \rightarrow 0} \sqrt{2\pi r} \sigma_\theta \quad (A.5)$$

$$K_{II} = \lim_{r \rightarrow 0} \sqrt{2\pi r} \tau_{r\theta} \quad (A.6)$$

$$K_{III} = \lim_{r \rightarrow 0} \sqrt{2\pi r} \tau_{\theta z} \quad (A.7)$$

## Appendix B

The solution for the blunt V-notches is not exact but represents the first term in a series perturbing the pointed notch solution. (7)

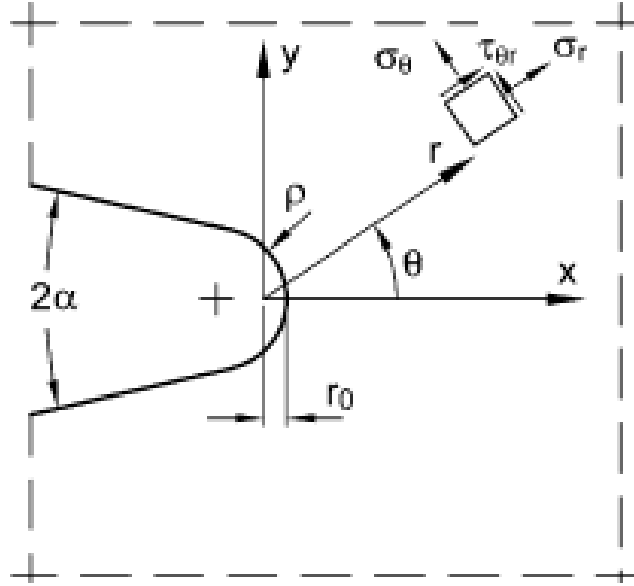


FIGURE 52 IN-PLANE NOTCH STRESS COMPONENTS AT THE ROUNDED V-NOTCH (7)

$$\begin{aligned}
 \begin{Bmatrix} \sigma_\theta \\ \sigma_r \\ \tau_{r\theta} \end{Bmatrix}_1 &= \frac{1}{\sqrt{2\pi}} \frac{r^{\lambda_1-1} K_1}{(1 + \lambda_1) + \chi_1(1 - \lambda_1)} \\
 &\times \left[ \begin{Bmatrix} (1 + \lambda_1) \cos(1 - \lambda_1)\theta \\ (3 - \lambda_1) \cos(1 - \lambda_1)\theta \\ (1 - \lambda_1) \sin(1 - \lambda_1)\theta \end{Bmatrix} + \chi_1(1 - \lambda_1) \begin{Bmatrix} \cos(1 + \lambda_1)\theta \\ -\cos(1 + \lambda_1)\theta \\ \sin(1 + \lambda_1)\theta \end{Bmatrix} \right] \\
 &+ \left( \frac{r}{r_0} \right)^{\mu_1 - \lambda_1} [(3 - \lambda_1) - \chi_1(1 - \lambda_1)] \begin{Bmatrix} \cos(1 + \mu_1)\theta \\ -\cos(1 + \mu_1)\theta \\ \sin(1 + \mu_1)\theta \end{Bmatrix} \quad (B.1)
 \end{aligned}$$

$$\begin{aligned}
\begin{Bmatrix} \sigma_\theta \\ \sigma_r \\ \tau_{r\theta} \end{Bmatrix}_2 &= \frac{1}{\sqrt{2\pi}} \frac{r^{\lambda_2-1} K_2}{(1 + \lambda_2) + \chi_2(1 - \lambda_2)} \\
&\times \left[ \begin{Bmatrix} -(1 + \lambda_2) \cos(1 - \lambda_2)\theta \\ -(3 - \lambda_2) \cos(1 - \lambda_2)\theta \\ (1 - \lambda_2) \sin(1 - \lambda_2)\theta \end{Bmatrix} + \chi_2(1 - \lambda_2) \begin{Bmatrix} -\sin(1 + \lambda_2)\theta \\ \sin(1 + \lambda_2)\theta \\ \cos(1 + \lambda_2)\theta \end{Bmatrix} \right] \\
&- \left( \frac{r}{r_0} \right)^{\mu_2 - \lambda_2} [(1 - \lambda_2) + \chi_2(1 + \lambda_2)] \begin{Bmatrix} \sin(1 + \mu_2)\theta \\ -\sin(1 + \mu_2)\theta \\ \cos(1 + \mu_2)\theta \end{Bmatrix} \quad (B.2)
\end{aligned}$$

The NSIFs  $K_1$  and  $K_2$  are determined for  $r \rightarrow 0$ . So for mode I and II the next expressions can be stated

$$\begin{Bmatrix} \sigma_\theta \\ \sigma_r \\ \tau_{r\theta} \end{Bmatrix}_{\rho \neq 0} = \begin{Bmatrix} \sigma_\theta \\ \sigma_r \\ \tau_{r\theta} \end{Bmatrix}_{\rho = 0} + \frac{1}{\sqrt{2\pi}} \frac{K_1}{r_0^{1-\lambda_1}} \left( \frac{r}{r_0} \right)^{\mu_1-1} \frac{(3 - \lambda_1) - \chi_1(1 - \lambda_1)}{(1 + \lambda_1) + \chi_1(1 - \lambda_1)} \begin{Bmatrix} \cos(1 + \mu_1)\theta \\ -\cos(1 + \mu_1)\theta \\ \sin(1 + \mu_1)\theta \end{Bmatrix} \quad (B.3)$$

$$\begin{Bmatrix} \sigma_\theta \\ \sigma_r \\ \tau_{r\theta} \end{Bmatrix}_{\rho \neq 0} = \begin{Bmatrix} \sigma_\theta \\ \sigma_r \\ \tau_{r\theta} \end{Bmatrix}_{\rho = 0} + \frac{1}{\sqrt{2\pi}} \frac{K_2}{r_0^{1-\lambda_2}} \left( \frac{r}{r_0} \right)^{\mu_2-1} \begin{Bmatrix} \sin(1 + \mu_2)\theta \\ -\sin(1 + \mu_2)\theta \\ -\cos(1 + \mu_2)\theta \end{Bmatrix} \quad (B.4)$$

The out-of-plane shear stresses are derived in the following form, separated into antisymmetrical (subscript a) and symmetrical (subscript s) parts in the  $r - \theta$  coordinate system

$$\begin{Bmatrix} \tau_{rz} \\ \tau_{\theta z} \end{Bmatrix} = \frac{K_{3\rho}^{(a)}}{\sqrt{2\pi}} r^{\lambda_a-1} \begin{Bmatrix} \sin \lambda_a \theta \\ \cos \lambda_a \theta \end{Bmatrix} + \frac{K_{3\rho}^{(s)}}{\sqrt{2\pi}} r^{\lambda_s-1} \begin{Bmatrix} \cos \lambda_s \theta - (r/r_0)^{\mu_s-\lambda_s} \cos \mu_s \theta \\ -\sin \lambda_s \theta + (r/r_0)^{\mu_s-\lambda_s} \sin \mu_s \theta \end{Bmatrix} \quad (B.5)$$

Where the antimetric and symmetric eigenvalues are dependent on the notch opening angle  $2\alpha$  expressed by the parameter  $q$

$$\lambda_a = \frac{1}{q}, \quad \lambda_s = \frac{2}{q}, \quad \mu_s = \frac{1}{q}, \quad q = \frac{2\pi - 2\alpha}{\pi} \quad (B.6)$$

The generalized NSIFs  $K_{3\rho}^a$  and  $K_{3\rho}^s$  are determined from the stresses in the bisector plane ( $\theta = 0$ ) of the blunt V-notch

$$K_{3\rho}^{(a)} = \lim_{r \rightarrow r_{0+}} \sqrt{2\pi} [r^{1-\lambda_a} \tau_{\theta z}(r, 0)] \quad (B.7)$$

$$K_{3\rho}^{(s)} = \lim_{r \rightarrow r_{0+}} \sqrt{2\pi} \left[ \frac{r^{1-\lambda_s} \tau_{rz}(r, 0)}{1 - (r/r_0)^{\mu_s - \lambda_s}} \right] \quad (B.8)$$



## Appendix C

In the presence of a sharp V-shaped notch, the stress distributions of symmetric type with respect to the angle bisector (mode I) are those calculated for the N-SIF.

By using the superposition effect principle, the stress distributions in the neighborhood of the notch tip can be given as follows (9):

$$\sigma_{ij}(r, \theta) = r^{\lambda_1-1} K_1 \begin{vmatrix} \tilde{\sigma}_{\theta\theta}^{(1)} & \tilde{\sigma}_{r\theta}^{(1)} & 0 \\ \tilde{\sigma}_{\theta r}^{(1)} & \tilde{\sigma}_{rr}^{(1)} & 0 \\ 0 & 0 & \tilde{\sigma}_{zz}^{(1)} \end{vmatrix} + r^{\lambda_2-1} K_2 \begin{vmatrix} \tilde{\sigma}_{\theta\theta}^{(2)} & \tilde{\sigma}_{r\theta}^{(2)} & 0 \\ \tilde{\sigma}_{\theta r}^{(2)} & \tilde{\sigma}_{rr}^{(2)} & 0 \\ 0 & 0 & \tilde{\sigma}_{zz}^{(2)} \end{vmatrix} \quad (C.1)$$

And by substituting in the expression of the SED the explicit expressions for stresses, one obtains:

$$W(r, \theta) = W_1(r, \theta) + W_2(r, \theta) + W_{12}(r, \theta) \quad (C.2)$$

In which

$$\begin{aligned} W_1(r, \theta) = & \frac{1}{2E} r^{2(\lambda_1-1)} K_1^2 \left[ \tilde{\sigma}_{\theta\theta}^{(1)2} + \tilde{\sigma}_{rr}^{(1)2} + \tilde{\sigma}_{zz}^{(1)2} \right. \\ & \left. - 2\nu \left( \tilde{\sigma}_{\theta\theta}^{(1)} \tilde{\sigma}_{rr}^{(1)} + \tilde{\sigma}_{\theta\theta}^{(1)} \tilde{\sigma}_{zz}^{(1)} + \tilde{\sigma}_{rr}^{(1)} \tilde{\sigma}_{zz}^{(1)} \right) + 2(1+\nu) \tilde{\sigma}_{r\theta}^{(1)2} \right] \end{aligned} \quad (C.3)$$

$$\begin{aligned} W_2(r, \theta) = & \frac{1}{2E} r^{2(\lambda_2-1)} K_2^2 \left[ \tilde{\sigma}_{\theta\theta}^{(2)2} + \tilde{\sigma}_{rr}^{(2)2} + \tilde{\sigma}_{zz}^{(2)2} \right. \\ & \left. - 2\nu \left( \tilde{\sigma}_{\theta\theta}^{(2)} \tilde{\sigma}_{rr}^{(2)} + \tilde{\sigma}_{\theta\theta}^{(2)} \tilde{\sigma}_{zz}^{(2)} + \tilde{\sigma}_{rr}^{(2)} \tilde{\sigma}_{zz}^{(2)} \right) + 2(1+\nu) \tilde{\sigma}_{r\theta}^{(2)2} \right] \end{aligned} \quad (C.4)$$

$$\begin{aligned} W_{12}(r, \theta) = & \frac{1}{E} r^{\lambda_1+\lambda_2-2} K_1 K_2 \left[ \tilde{\sigma}_{\theta\theta}^{(1)} \tilde{\sigma}_{\theta\theta}^{(2)} + \tilde{\sigma}_{rr}^{(1)} \tilde{\sigma}_{rr}^{(2)} + \tilde{\sigma}_{zz}^{(1)} \tilde{\sigma}_{zz}^{(2)} \right. \\ & - \nu \left( \tilde{\sigma}_{\theta\theta}^{(1)} \tilde{\sigma}_{rr}^{(2)} + \tilde{\sigma}_{\theta\theta}^{(1)} \tilde{\sigma}_{zz}^{(2)} + \tilde{\sigma}_{rr}^{(1)} \tilde{\sigma}_{\theta\theta}^{(2)} + \tilde{\sigma}_{rr}^{(1)} \tilde{\sigma}_{zz}^{(2)} + \tilde{\sigma}_{zz}^{(1)} \tilde{\sigma}_{\theta\theta}^{(2)} \right. \\ & \left. \left. + \tilde{\sigma}_{zz}^{(1)} \tilde{\sigma}_{rr}^{(2)} \right) + 2(1+\nu) \tilde{\sigma}_{r\theta}^{(1)} \tilde{\sigma}_{r\theta}^{(2)} \right] \end{aligned} \quad (C.5)$$

The elastic deformation energy in a region of radius  $R$  around the notch tip is

$$E(R) = \int_A W dA = \int_0^R \int_{-\gamma}^{+\gamma} [W_1(r, \theta) + W_2(r, \theta) + W_{12}(r, \theta)] r dr d\theta \quad (C.6)$$

Since the integration field is symmetric with respect to the notch bisector, the contribution of  $W_{12}$  vanishes. As a consequence:

$$E(R) = E_1(R) + E_2(R) = \frac{1}{E} \frac{I_1(\gamma)}{4\lambda_1} K_1^2 R^{2\lambda_1} + \frac{1}{E} \frac{I_2(\gamma)}{4\lambda_2} K_2^2 R^{2\lambda_2} \quad (C.7)$$

where integrals  $I_1$  and  $I_2$  are:

$$I_1(\gamma) = \int_{-\gamma}^{+\gamma} \left( \tilde{\sigma}_{\theta\theta}^{(1)2} + \tilde{\sigma}_{rr}^{(1)2} + \tilde{\sigma}_{zz}^{(1)2} - 2\nu \left( \tilde{\sigma}_{\theta\theta}^{(1)} \tilde{\sigma}_{rr}^{(1)} + \tilde{\sigma}_{\theta\theta}^{(1)} \tilde{\sigma}_{zz}^{(1)} + \tilde{\sigma}_{rr}^{(1)} \tilde{\sigma}_{zz}^{(1)} \right) + 2(1 + \nu) \tilde{\sigma}_{r\theta}^{(1)2} \right) d\theta \quad (C.8)$$

$$I_2(\gamma) = \int_{-\gamma}^{+\gamma} \left( \tilde{\sigma}_{\theta\theta}^{(2)2} + \tilde{\sigma}_{rr}^{(2)2} + \tilde{\sigma}_{zz}^{(2)2} - 2\nu \left( \tilde{\sigma}_{\theta\theta}^{(2)} \tilde{\sigma}_{rr}^{(2)} + \tilde{\sigma}_{\theta\theta}^{(2)} \tilde{\sigma}_{zz}^{(2)} + \tilde{\sigma}_{rr}^{(2)} \tilde{\sigma}_{zz}^{(2)} \right) + 2(1 + \nu) \tilde{\sigma}_{r\theta}^{(2)2} \right) d\theta \quad (C.9)$$

The area on which the integration is carried out is expressed by (1.31)

The elastic deformation energy, averaged on the area  $A$ , turns out to be:

$$\bar{W} = \frac{E(R)}{A(R)} = \frac{1}{E} e_1 K_1^2 R^{2(\lambda_1-1)} + \frac{1}{E} e_2 K_2^2 R^{2(\lambda_2-1)} \quad (C.10)$$

Where  $e_1$  and  $e_2$  are expressed by (1.29) and (1.30) respectively.

## Appendix D

Considering a set with  $n$  values  $y_1, y_2, \dots, y_n$  associated to  $n$  predicted values  $f_1, f_2, \dots, f_n$  the residuals are defined as  $e_1 = y_i - f_i$  and the mean is:

$$\bar{y} = \frac{1}{n} \sum_{i=1}^n y_i \quad (D.1)$$

The total sum of squares is:

$$SS_{\text{tot}} = \sum_i (y_i - \bar{y})^2 \quad (D.2)$$

The regression sum of squares is:

$$SS_{\text{reg}} = \sum_i (f_i - \bar{y})^2 \quad (D.3)$$

The sum of squares of residuals is:

$$SS_{\text{res}} = \sum_i (y_i - f_i)^2 = \sum_i e_i^2 \quad (D.4)$$

Finally R-squared is define as:

$$R^2 \equiv 1 - \frac{SS_{\text{res}}}{SS_{\text{tot}}} \quad (D.5)$$

$R^2$  is a value that represents the goodness of fit and it expresses how well the regression approximate the real data points. An  $R^2$  of 1 indicates that the regression predictions perfectly fit the data. Values of  $R^2$  outside the range 0 to 1 can occur when the model fits the data worse than a horizontal hyperplane. This would occur when the wrong model was chosen, or nonsense constraints were applied.

# Bibliography

1. *Stephens, Ralph ,Fuchs, Henry ,Stephens, Robert, Metal Fatigue in Engineering, 2000.*
2. *Lüpfert, H.P.; Spies, H.J., Fatigue strength of heat-treated steel under static multiaxial compression stress, Adv. Eng. Mater., 2004.*
3. *Pallarés-Santasmartas L., Albizuri J., Avilés A., Avilés R., Mean Stress Effect on the Axial Fatigue Strength of DIN 34CrNiMo6 Quenched and Tempered Steel, MDPI, 2018.*
4. *Goodman J., Mechanics Applied to Engineering, Longmans Green, 1899.*
5. *Haigh B.P., Elastic and Fatigue Fracture in Metals. Metal Ind., 1922.*
6. *Suresh, S., Fatigue of Materials, Cambridge University Press, 1998.*
7. *Radaj D. Advanced Methods of Fatigue Assessment, Springer-Verlag Berlin Heidelberg 2013.*
8. *Lazzarin P, Berto F, Gomez F J, Zappalorto M., Some advantages derived from the use of the strain energy density over a control volume in fatigue strength assessments of welded joints, International Journal of Fatigue, 2008.*
9. *Lazzarin P, Zambardi R., A finite-volume-energy based approach to predict the static and fatigue behavior of components with sharp V-shaped notches, International Journal of Fracture, 2001.*
10. *Poutiainen I., Marquis G., A fatigue assessment method based on welded stress, Int J Fatigue, 2006.*
11. *Lazzarin P, Berto F, Zappalorto M., Rapid calculations of notch stress intensity factors based on averaged strain energy density from coarse meshes: Theoretical bases and applications, International Journal of Fatigue, 2010.*

12. *Livieri P, Lazzarin P., Fatigue strength of steel and aluminium welded joints based on generalised stress intensity factors and local strain energy values, Int J Fract, 2005.*
13. *Paris P., Erdogan F., A Critical Analysis of Crack Propagation Laws,ASME,1963.*
14. *Marco Evangelos Biancolini, Propagazione di cricche di fatica in componenti,Phd Thesis,2015.*
15. *Peng Y.,Wang G.,Zhu T.,Pan S., Rong Y., Dynamic Mechanical Behaviors of 6082-T6 Aluminum Alloy, Hindawi Publishing Corporation,2013.*
16. *José A.F.O. Correia, Abílio M.P. De Jesusa, Ana S.F. Alvesa, Grzegorz Lesiukb,Paulo J.S. Tavaresa, Pedro M.G.P. Moreira, Fatigue crack growth behaviour of the 6082-T6 aluminium using CT specimens with distinct notches, 21st European Conference on Fracture. 2016.*
17. *Ince A., A generalized mean stress correction model based on distortional strain,International Journal of Fatigue,2017.*
18. *Badibanga R., Miranda T., Rocha P., Ferreira J.,da Silva C., Araújo J., The effect of mean stress on the fatigue behaviour of overhead conductor function of the H/w parameter, MATEC Web of Conferences, 2018.*